nature cell biology

Secreted IGFBP5 mediates mTORC1-dependent feedback inhibition of IGF-1 signalling

Ming Ding[1], Richard K. Bruick[1] and Yonghao Yu[1,2]

The PI(3)K–Akt–mTORC1 pathway is a highly dynamic network that is balanced and stabilized by a number of feedback inhibition loops[1,2]. Specifically, activation of mTORC1 has been shown to lead to the inhibition of its upstream growth factor signalling. Activation of the growth factor receptors is triggered by the binding of their cognate ligands in the extracellular space. However, whether secreted proteins contribute to the mTORC1-dependent feedback loops remains unclear. We found that cells with hyperactive mTORC1 secrete a protein that potently inhibits the function of IGF-1. Using a large-scale, unbiased quantitative proteomic platform, we comprehensively characterized the rapamycin-sensitive secretome in *TSC2*$^{-/-}$ mouse embryonic fibroblasts, and identified IGFBP5 as a secreted, mTORC1 downstream effector protein. IGFBP5 is a direct transcriptional target of HIF1, which itself is a known mTORC1 target[3]. IGFBP5 is a potent inhibitor of both the signalling and functional outputs of IGF-1. Once secreted, IGFBP5 cooperates with intracellular branches of the feedback mechanisms to block the activation of IGF-1 signalling. Finally, IGFBP5 is a potential tumour suppressor, and the proliferation of *IGFBP5*-mutated cancer cells is selectively blocked by IGF-1R inhibitors.

The evolutionarily conserved serine/threonine kinase mTOR (mechanistic target of rapamycin) is a central regulator of cell growth and proliferation. mTOR is distributed into two complexes, mTORC1 and mTORC2. The upstream inputs regulating mTORC1 have been extensively characterized. Multiple signals (for example, from growth factors and tumour-promoting phorbol esters) converge on the heterodimeric TSC1/2 (tuberous sclerosis complex) protein complex to regulate the activation of mTORC1, in a Rheb-dependent manner[1,2]. In addition, mTORC1 activity is also under the tight control of cellular amino acid levels[4].

The best-known mTORC1 substrates are the eIF4E-binding proteins (4EBPs) and the ribosomal protein S6 kinases (S6K), both of which are known to regulate protein synthesis[5]. Recently, we and others have used large-scale quantitative mass spectrometry experiments to comprehensively characterize the mTORC1-regulated phosphoproteome[6–8]. These studies measured, on a global level, the changes in protein phosphorylation on rapamycin treatment, and in so doing, identified additional mTORC1 substrates (for example, growth factor receptor-bound protein 10, GRB10; refs 6,8).

Downstream effector proteins of mTORC1 are known to communicate with its upstream regulators (for example, receptor tyrosine kinases, RTKs), through various feedback loops[9]. These feedback mechanisms play a critical role in maintaining the stability of the entire network. They also have great significance in a variety of diseases. In particular, mTORC1 is hyperactivated in many human cancers, as a result of mutations of upstream oncogenes and tumour suppressors (for example, *PI3K*, *PTEN*, *Akt*, *TSC1/2*, and so on)[2], or mTOR itself[10]. In most of the cases, rapamycin or mTOR kinase inhibitors, however, fail to kill tumour cells[11].

Recent studies have suggested multiple mechanisms of rapamycin resistance. For example, tumours could develop mTOR mutations that prevent the binding of rapamycin to the protein by means of steric hindrance[12]. In addition, rapamycin resistance could also stem from the relief of mTORC1-mediated feedback inhibition loops[2]. Specifically, mTORC1 inhibition could activate growth factor signalling, providing an alternative means of promoting cell survival and proliferation, under these mTORC1-repressed conditions[13]. A number of studies have demonstrated that the feedback mechanisms involve mTORC1/S6K targeting growth factor receptors[14,15], proteins that bind to RTKs (for example, IRS1 (refs 16,17) and GRB10 (refs 6,8)) and more downstream mTORC2 (through phosphorylation of mSin1; refs 18,19). These feedback mechanisms, however, only partially account for the mTORC1-dependent inhibitory activity towards growth factor signalling. We realize that the above-mentioned molecules (that is, GRB10, IRS1 and mSin1) are intracellular proteins. However, activation of RTKs is triggered by the binding of their cognate ligands in the extracellular space. Whether secreted

[1]Department of Biochemistry, University of Texas Southwestern Medical Center, 5323 Harry Hines Boulevard, Dallas, Texas 75235, USA.
[2]Correspondence should be addressed to Y.Y. (e-mail: yonghao.yu@utsouthwestern.edu)

Received 11 February 2015; accepted 8 January 2016; published online 8 February 2016; DOI: 10.1038/ncb3311

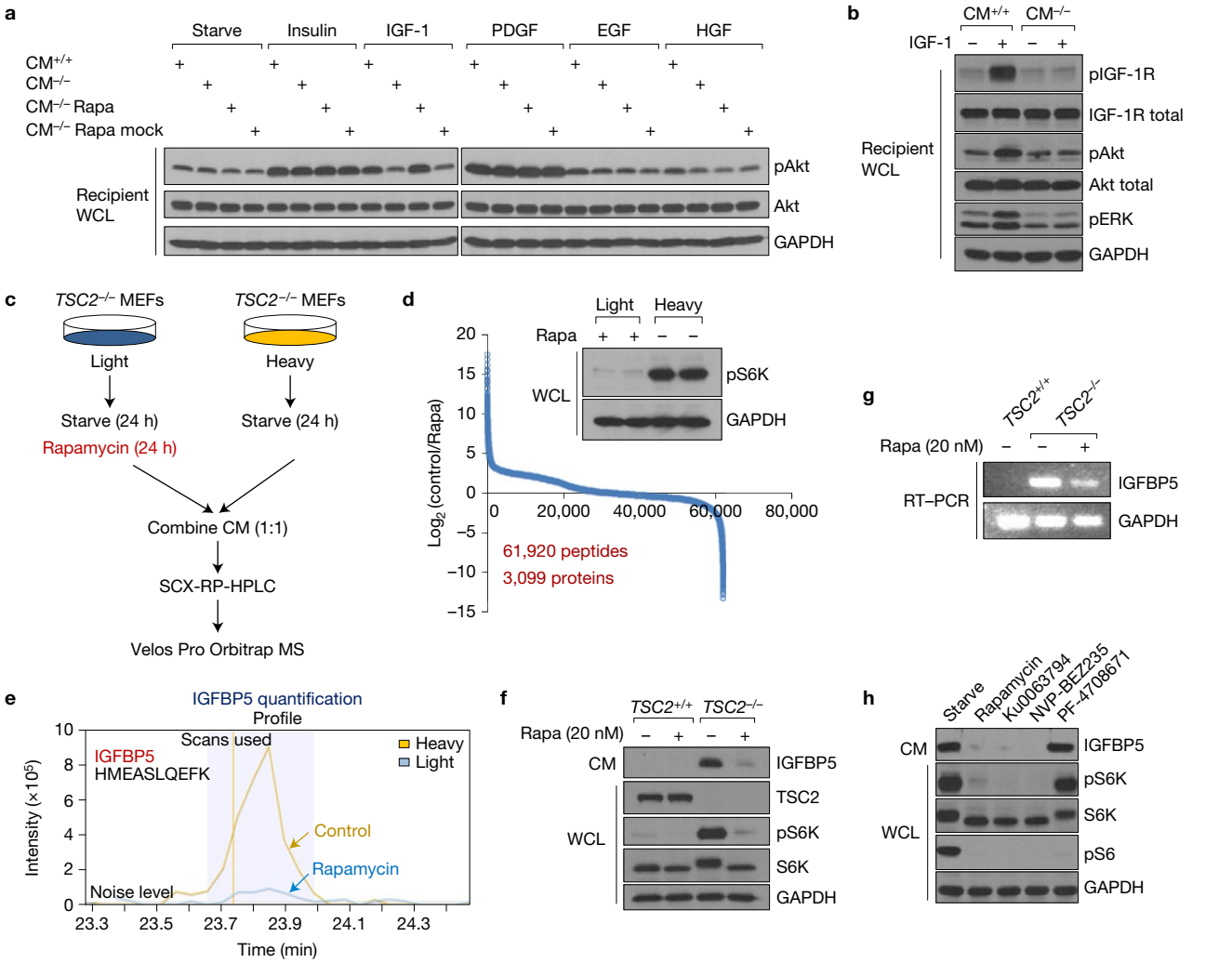

Figure 1 Cells with hyperactivated mTORC1 secrete a protein factor(s) that blocks IGF-1 signalling. (**a**) CM (conditioned media) was collected from *TSC2*$^{+/+}$ MEFs (CM$^{+/+}$) or *TSC2*$^{-/-}$ MEFs (CM$^{-/-}$), mixed with the indicated growth factor, and then incubated with wild-type MEFs (designated as 'recipient cells') for 10 min. CM that was not mixed with any growth factors is indicated as 'starve'. CM was also collected from *TSC2*$^{-/-}$ MEFs that had been treated with 20 nM rapamycin for 24 h (CM$^{-/-}$ Rapa). As a control experiment, CM from *TSC2*$^{-/-}$ cells were collected first, and then mixed with rapamycin (CM$^{-/-}$ Rapa mock). For site-specific phosphorylation, pAkt(S473) levels were analysed. Growth factor concentrations are: insulin, 100 nM; IGF-1, 40 ng ml^{-1}; PDGF, 50 ng ml^{-1}; EGF, 50 ng ml^{-1}; and HGF, 50 ng ml^{-1}. WCL, whole-cell lysate. (**b**) CM from *TSC2*$^{-/-}$ MEFs is able to block the activation of the IGF-1 signalling pathway. Experiments were performed as in **a**. pIGF-1R(Y1135/1136), pAkt(S473) and pERK(T202/Y204) levels were analysed. (**c**) A general schematic of the quantitative secretomic platform. SCX-RP-HPLC, strong-cation-exchange reversed-phase high-performance liquid chromatography. (**d**) Ratio distribution of the identified peptides (a total of 61,920 from 3,099 proteins). Ratio (control/rapamycin-treated) distribution of these peptides is shown on a $\log_2$ scale. Light and heavy lysates were also subject to immunoblotting analysis for pS6K(T389) levels. (**e**) Extracted ion chromatogram of the light (rapamycin-treated, blue) and heavy (control, yellow) ions of an IGFBP5 peptide (HMEASLQEFK). (**f**) CM from *TSC2*$^{-/-}$ MEFs, but not *TSC2*$^{+/+}$ MEFs, contains high levels of IGFBP5. Cells were starved for 24 h, after which CM was collected. When indicated, cells were also treated with rapamycin (20 nM for 24 h). CM and WCL of these cells were analysed by immunoblotting for pS6K(T389) levels. (**g**) IGFBP5 expression is regulated by mTORC1 at the transcription level. Total RNA was extracted from *TSC2*$^{+/+}$ MEFs, *TSC2*$^{-/-}$ MEFs, or *TSC2*$^{-/-}$ MEFs that had been treated with 20 nM rapamycin for 24 h, and was analysed. (**h**) Treatment of *TSC2*$^{-/-}$ MEFs by rapamycin (20 nM), Ku0063794 (1 μM) and NVP-BEZ235 (500 nM), but not an S6K inhibitor (PF-4708671, 10 μM), led to downregulation of IGFBP5 in CM. For site-specific phosphorylation, pS6K(T389) and pS6(S235/236) levels were analysed. Unprocessed original scans of blots are shown in Supplementary Fig. 6.

proteins contribute to mTORC1-dependent feedback mechanisms is unknown.

To address this question, we serum-starved a pair of isogenic *TSC2*$^{+/+}$ and *TSC2*$^{-/-}$ mouse embryonic fibroblasts (MEFs) in DMEM for 24 h, and collected their conditioned media (CM). Loss of *TSC2* disengages mTORC1 from the upstream inputs, resulting in its constitutive activation, even in serum-free media[8,20]. As a result, these cells are resistant to serum deprivation-induced apoptosis (Supplementary Fig. 1A). They also possess potent mTORC1-dependent feedback loops (Supplementary Fig. 1B).

We mixed the corresponding CM with various growth factors, including insulin, IGF-1, PDGF, EGF and HGF. These CM samples were then incubated with separate plates of wild-type MEFs (Fig. 1a). We found that IGF-1 was able to activate IGF-1R and Akt in recipient

cells only when it was mixed with CM from $TSC2^{+/+}$ cells, but not with that from $TSC2^{-/-}$ cells (Fig. 1a,b). Activity of the other growth factors was not affected by $TSC2^{-/-}$ CM. Remarkably, this IGF-1-inhibitory activity was abrogated in CM from $TSC2^{-/-}$ cells that had been treated with rapamycin for 24 h (Fig. 1a). Here, because this CM contained rapamycin, there was also a possibility that the observed restoration of IGF-1 signalling was a direct effect of rapamycin on the recipient cells. We performed control experiments where we collected CM from $TSC2^{-/-}$ cells, and then mixed it with rapamycin. We found that this mock-treatment media retained the ability to inhibit IGF-1 (Fig. 1a). The simplest hypothesis that is consistent with these observations would be that cells with hyperactive mTORC1 secrete a factor(s) that is able to block the function of IGF-1.

$TSC2^{-/-}$ CM that had been heated to 95 °C completely lost its ability to inhibit IGF-1, suggesting that this factor might be a protein (Supplementary Fig. 1C). This experiment also ruled out the possibility that the observed effect was because mTORC1 activation inhibits the accumulation of an IGF-1-potentiating protein (in which case, heating the CM from $TSC2^{-/-}$ cells would not affect its ability to modulate IGF-1 signalling).

We sought to identify this mTORC1-regulated, secreted protein factor(s) that has IGF-1-inhibitory activity. Mass spectrometric analysis of secreted proteins, however, is technically challenging, owing to their often exceedingly low abundances[21]. By coupling multi-dimensional high-performance liquid chromatography separation with a Velos Pro Orbitrap mass spectrometer, we established a high-sensitivity mass spectrometry platform for comprehensive secretomic analysis (Fig. 1c).

Although uncontrolled activation of mTORC1 is the best studied and the predominant consequence of *TSC2* loss, there could be mTORC1-independent functions from *TSC2* loss. These functions might also regulate the expression of secreted proteins. We therefore focused on identifying secreted proteins whose expression was altered as a result of rapamycin treatment. We used the SILAC (stable isotope labelling by amino acids in cell culture) approach[8,22] as the quantification method (Fig. 1c). Both light and heavy $TSC2^{-/-}$ MEFs were serum-deprived for 24 h, during which light cells were rapamycin-treated (Fig. 1d). CM from the light and heavy cells were collected, combined (at a 1:1 ratio at the protein level) and analysed by the above-mentioned quantitative secretomic platform.

From this SILAC CM sample, we identified and quantified a total of 61,920 peptides from 3,099 proteins (peptide false discovery rate = 0.27%; Fig. 1d and Supplementary Fig. 1D and Supplementary Tables 4–7). mTORC1 inhibition leads to a marked change in the secretome. Specifically, 355 and 145 proteins showed a decrease and increase in their abundances, by at least 32-fold, respectively, after rapamycin treatment (Fig. 1d). For example, the abundance of fibroblast growth factor 21 (FGF21) markedly decreased after rapamycin treatment (Supplementary Fig. 1E). FGF21 is a secreted hormone whose expression is known to be regulated by mTORC1 (ref. 23). The identification of this known mTORC1 downstream target in the extracellular space validates the robustness of our quantitative secretomic approach.

As rapamycin treatment abrogated the expression of the IGF-1-inhibitory protein (Fig. 1a), we focused our follow-up analysis on proteins whose abundances decreased as a result of mTORC1 inhibition. Gene ontology (cellular compartment) analysis of these proteins showed that they were enriched for extracellular matrix proteins ($P = 6.5 \times 10^{-10}$; Supplementary Fig. 2A). Intriguingly, one of the enriched molecular function categories was growth factor binding proteins ($P = 1.7 \times 10^{-4}$; Supplementary Fig. 2B). In particular, the level of IGFBP5 (IGF binding protein 5) decreased markedly (by approximately 68-fold; similar change was found in the replicate SILAC experiment) after rapamycin treatment (Fig. 1e and Supplementary Fig. 1F).

IGFBPs are secreted proteins that are known to bind to circulating IGF-1 (ref. 24). Interestingly, another member of the IGFBP family, IGFBP3, has recently been shown to be regulated by mTORC2 (ref. 25). We confirmed that $TSC2^{-/-}$ contained high levels of IGFBP5 at both the protein (in CM) and messenger RNA levels (Fig. 1f,g). Conversely, this protein was virtually absent in CM from $TSC2^{+/+}$ MEFs. To rule out the possibility that this observation is due to artefacts resulting from *in vitro* culturing of these isogenic cells, we generated *TSC2*-reconstituted cells by introducing *TSC2* back into $TSC2^{-/-}$ MEFs. Indeed, these 'wild-type' cells also contained undetectable levels of secreted IGFBP5 (Supplementary Fig. 1G).

Inhibition of mTORC1 in $TSC2^{-/-}$ MEFs by either rapamycin or mTOR kinase inhibitors (Ku0063794 and NVP-BEZ235; ref. 8) resulted in a marked decrease of IGFBP5 (Fig. 1f–h). In contrast, treatment of these cells with an S6K inhibitor, PF-4708671 (ref. 26), had no effect on IGFBP5 levels (Fig. 1h). These results indicate that mTORC1 itself, rather than S6K, regulates the expression of IGFBP5. mTORC1 also regulates the expression of IGFBP5 in other cell lines (RT-4 and MCF7, Supplementary Fig. 1H,I).

As the mRNA level of IGFBP5 positively correlated with mTORC1 activity (Fig. 1g), we reasoned that transcription regulation might contribute to mTORC1-dependent IGFBP5 expression. Several transcription factors are known to function downstream of mTORC1, including sterol regulatory element-binding protein (SREBP), c-Myc and HIF1 (hypoxia-inducible factor 1; refs 27–29). HIF1 is of particular interest because it modulates the expression of a number of secreted proteins (for example, VEGF; ref. 30). Activation of mTORC1 promotes the synthesis of HIF1α, specifically through enhancing the translation of its mRNA that contains long and structured 5′-UTRs (ref. 3).

Consistent with previous studies[27], we found that rapamycin treatment markedly lowered the expression of HIF1α and, concomitantly, IGFBP5 in $TSC2^{-/-}$ MEFs (Fig. 2a). A similar decrease in IGFBP5 was observed when HIF1α was knocked down using RNAi (RNA interference) in $TSC2^{-/-}$ MEFs (Fig. 2b,c) and RT-4 cells (Fig. 2d). We found that HIF1 was also sufficient for IGFBP5 expression. Specifically, treatment of RT-4 cells with a hypoxia-mimetic agent, $CoCl_2$ (ref. 30), led to robust accumulation of HIF1α and IGFBP5 (in CM) (Fig. 2e). Importantly, co-treatment of $CoCl_2$ and rapamycin suppressed HIF1α and IGFBP5 expression to levels even lower than $CoCl_2$-untreated samples (Fig. 2f,g), suggesting a dominant effect from mTORC1 inhibition. IGFBP5 expression is no longer sensitive to rapamycin treatment in an ectopic expression system (the construct does not contain the highly structured 5′-UTR of HIF1α), suggesting that the effect of rapamycin on IGFBP5 expression is dependent on mTORC1-mediated translation of HIF1α (Fig. 2h).

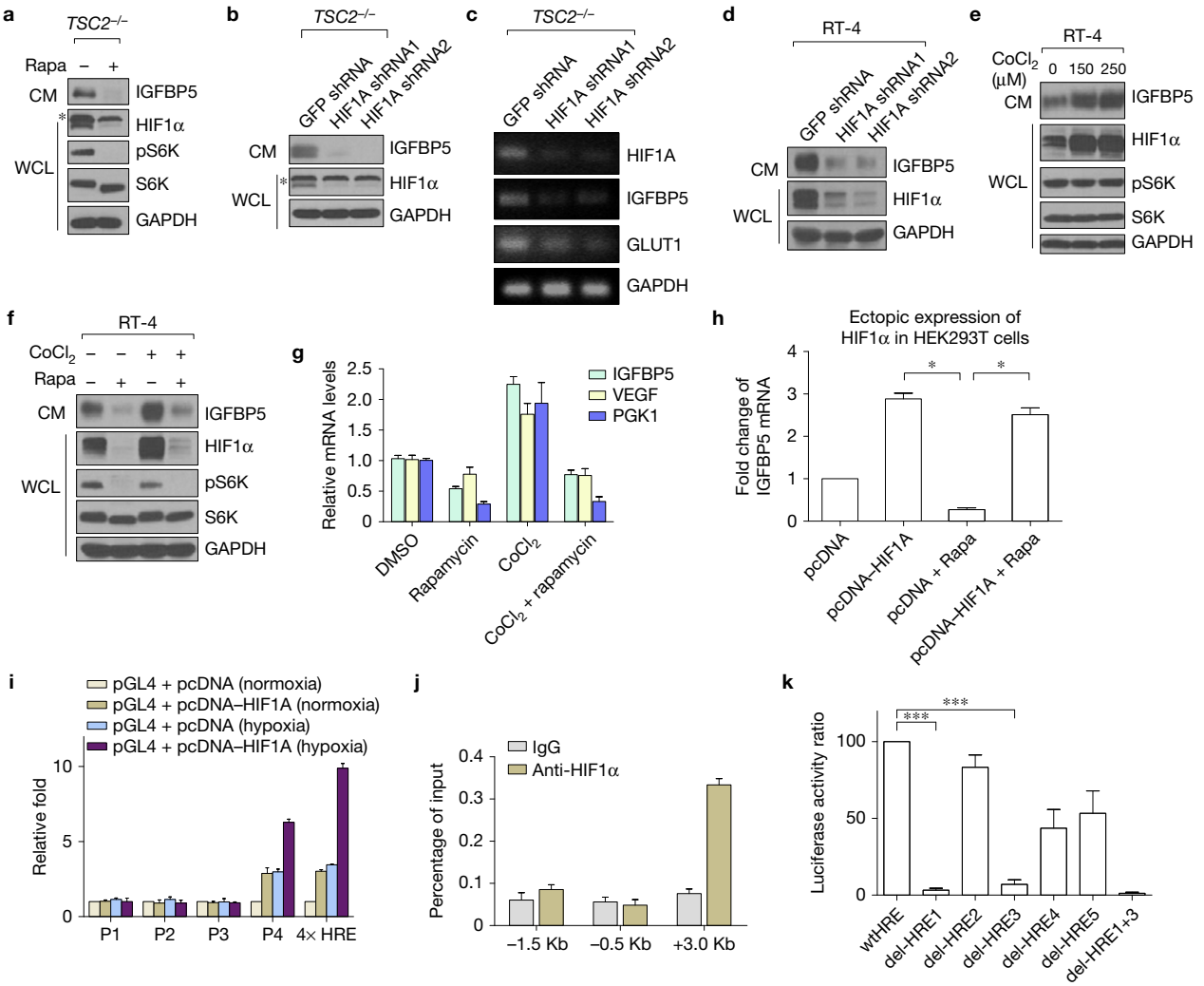

Figure 2 Expression of IGFBP5 is transcriptionally regulated by HIF1α. (**a**) Rapamycin treatment (20 nM, 24 h) of *TSC2*$^{-/-}$ MEFs led to a concurrent downregulation of HIFα (in WCL) and IGFBP5 (in CM). The asterisk indicates a nonspecific band. For site-specific phosphorylation, pS6K(T389) levels were analysed. (**b**,**c**) RNAi-mediated knockdown of HIFα in *TSC2*$^{-/-}$ MEFs led to downregulation of IGFBP5 at both protein (**b**) and mRNA (**c**) levels. GLUT1 is a known transcriptional target of HIFα, and was used as a positive control. The asterisk indicates a nonspecific band. (**d**) Knockdown of HIF1α in RT-4 cells led to a similar downregulation of IGFBP5 levels in CM. (**e**) Treating RT-4 cells with a hypoxic mimetic, $CoCl_2$ (24 h with the indicated concentrations), led to stabilization of HIF1α in WCL, and accumulation of IGFBP5 in CM. (**f**,**g**) Concurrent treatment of RT-4 cells with $CoCl_2$ (250 μM) and rapamycin (20 nM) abolished IGFBP5 expression at the protein (**f**) and mRNA (**g**) levels. $P < 0.05$ (two-way ANOVA test). $n = 3$ independent biological replicate experiments. Error bars represent s.d. (**h**) IGFBP5 expression is insensitive to mTORC1 inhibition (rapamycin at 20 nM, 24 h) in a HIF1α ectopic expression system. HEK293T cells were transfected with either a pcDNA–HIF1A or a control vector. IGFBP5 mRNA levels were determined by quantitative RT–PCR. $^{*}P < 0.05$ (two-tailed Student *t*-test). $n = 3$ independent biological replicate experiments; error bars represent s.d. (**i**) Luciferase reporter assays indicate that the first intron (designed as P4, see Supplementary Fig. 3) of the *IGFBP5* gene contains functional HREs. Luciferase activities were normalized to *Renilla* luciferase. Hypoxia was induced by growing the cells in a hypoxia chamber (1% O_2). A luciferase reporter construct containing 4× HRE (from Promega) was used as the positive control. $P < 0.001$ (two-way ANOVA test). $n = 3$ independent biological replicate experiments. Error bars represent s.d. (**j**) ChIP–qRT–PCR confirmation of the binding between HIF1α and the potential HREs in the P4 region. $P < 0.001$ (two-way ANOVA test). $n = 3$ independent biological replicate experiments. Error bars represent s.d. (**k**) Deletion of HRE1 and HRE3 (Supplementary Fig. 3) in the P4 region of the *IGFBP5* gene abolishes the binding of HIF1α in the luciferase assay. $^{***}P < 0.001$ (two-tailed Student *t*-test). $n = 3$ independent biological replicate experiments; error bars represent s.d. Unprocessed original scans of blots are shown in Supplementary Fig. 6.

To explore whether HIF1 directly regulates the transcription of *IGFBP5*, we screened a series of pGL4 luciferase reporter constructs harbouring inserts representing different regions of the *IGFBP5* gene (Supplementary Fig. 3). We found that the expression of one construct (pGL4–P4–luc) that carries a 300-base-pair (bp; from +2.9 Kb to +3.2 Kb) fragment downstream of the *IGFBP5* transcription start site in HEK293T cells led to a marked increase in luciferase activity, when these cells were co-transfected with a pcDNA3–HIF1A plasmid (Fig. 2i). These data suggest that there could be potential HIF-responsive elements (HREs) in this region of the *IGFBP5* gene. Chromatin immunoprecipitation–quantitative PCR (ChIP–qPCR) experiments then confirmed the existence of such HREs (Fig. 2j).

On the basis of the consensus binding motifs of HIF1 (5′-CGTG-3′; ref. 31), we identified a total of five potential HREs in this region

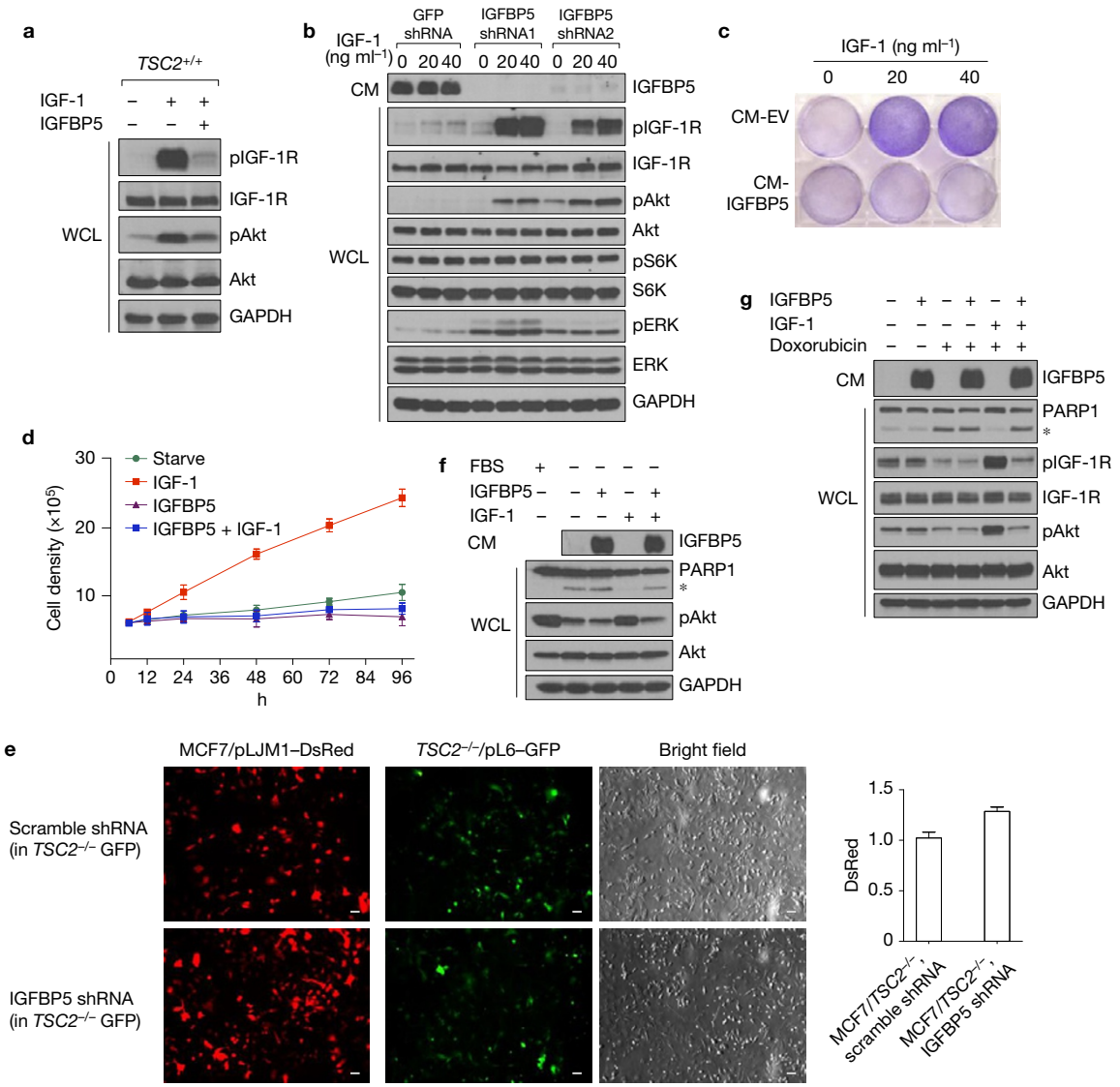

Figure 3 IGFBP5 is a potent inhibitor of IGF-1 signalling. (**a**) Addition of recombinant IGFBP5 (R&D Systems) to culture media blocks IGF-1-induced activation (20 ng ml^{-1}, 5 min) of IGF-1R (pIGF-1R(Y1135/1136)) and Akt (pAkt(S473)) in wild-type MEFs. (**b**) Knockdown of IGFBP5 in *TSC2*$^{-/-}$ MEFs led to strong activation of IGF-1R and its downstream kinases (Akt and ERK) in response to IGF stimulation. Cells were starved overnight, and were stimulated with IGF (20 ng ml^{-1}, 5 min). For site-specific phosphorylation, pIGF-1R(Y1135/1136), pAkt(S473), pS6K(T389) and pERK(T202/Y204) levels were analysed. (**c**,**d**) Addition of IGFBP5 to culture media blocked IGF-1-induced cell proliferation. MCF7 cells were starved, and were then treated with IGF-1 mixed with CM from HEK293T cells transfected with an empty vector (CM-EV), or an IGFBP5-expressing construct (CM-IGFBP5), respectively. Cells were stained by crystal violet (**c**) (after 48 h), or counted (**d**). $P < 0.001$ (two-way ANOVA test). $n = 9$ independent biological replicate experiments. Error bars represent s.d. (**e**) IGFBP5 secreted from *TSC2*$^{-/-}$ MEFs inhibits the growth of MCF7 cells in a co-culture system. MCF7 cells were labelled with red florescent protein (DsRed), and were grown with GFP-labelled *TSC2*$^{-/-}$ MEFs with either control knockdown or IGFBP5 knockdown. Cells were grown in DMEM supplemented with IGF-1 (40 ng ml^{-1}), with fluorescence signal intensities quantified for the green and red channels. $P < 0.05$ (two-tailed Student *t*-test). $n = 3$ independent biological replicate experiments. Error bars represent s.d. Scale bars, 40 μm. (**f**) The presence of IGF (40 ng ml^{-1}) in culture media protected cells from starvation-induced apoptosis. This effect, however, is blocked by the addition of IGFBP5. The asterisk indicates cleaved PARP1. CM from HEK293T cells transfected with an IGFBP5-expressing construct was used as the source of IGFBP5. For site-specific phosphorylation, pAkt(S473) levels were analysed. (**g**) The presence of IGF-1 in culture media protected cells from doxorubicin-induced (1 μM, 6 h) apoptosis. This effect was blocked by the addition of IGFBP5. MCF7 cells were starved overnight, and were treated with doxorubicin in the presence of IGF-1 (40 ng ml^{-1}) or IGF-1+IGFBP5. CM from HEK293T cells transfected with an IGFBP5-expressing construct was used as the source of IGFBP5. For site-specific phosphorylation, pIGF-1R(Y1135/1136) and pAkt(S473) levels were analysed. Unprocessed original scans of blots are shown in Supplementary Fig. 6.

(HRE1–HRE5, Supplementary Fig. 3). We found that the deletion of either HRE1 or HRE3 markedly lowered the binding of HIF1 in the luciferase assay. HIF1 completely lost its ability to recognize the IGFBP5 mutant that has been deleted for both HRE1 and HRE3, indicating that these two HREs are the most important sites for HIF1-dependent transcription regulation of IGFBP5 (Fig. 2k). Taken together, these data demonstrate that HIF1α regulates the transcription of IGFBP5 through directly binding to its HREs.

IGFBP5 is known to bind, with high affinity, to circulating IGFs (ref. 24). However, it remains controversial whether IGFBP5 impacts IGF-1 signalling in a positive or negative manner. IGFBP5 could block IGF-1 signalling by binding to, and sequestering it from interacting with IGF-1R (ref. 32). On the other side, IGFBP5 might also potentiate the function of IGF-1, presumably by better presenting IGF-1 to IGF-1R (ref. 33). We found that the addition of IGFBP5 to the media resulted in strong inhibition of IGF-1 signalling in wild-type MEFs (Fig. 3a). We found that IGFBP5 is also necessary for the IGF-1-inhibitory activity in $TSC2^{-/-}$ CM. $TSC2^{-/-}$ MEFs are characterized by a profound 'IGF-1-resistant' state, as indicated by their lack of response to IGF-1 (Fig. 3b). Intriguingly, depletion of IGFBP5 in $TSC2^{-/-}$ MEFs greatly sensitizes them to IGF-1 stimulation (Fig. 3b).

We next examined whether IGFBP5 also inhibits the functional outputs of IGF-1. We found that the addition of IGFBP5 to culture media completely blocked IGF-1-induced proliferation of MCF7 cells (Fig. 3c,d). As IGFBP5 is a secreted protein that functions in the extracellular space, it may also provide a 'non-cell autonomous' mechanism for mTORC1 to regulate the growth and proliferation of adjacent cells. We tested this hypothesis using a co-culture system. Specifically, MCF7 cells were labelled with red florescent protein (DsRed, RFP), and were grown with GFP-labelled $TSC2^{+/+}$ or $TSC2^{-/-}$ MEFs. Interestingly, the proliferation of MCF7 cells was markedly suppressed when they were co-cultured with $TSC2^{-/-}$ MEFs (Supplementary Fig. 4A), an effect that can be ascribed to IGFBP5 (Fig. 3e).

We investigated whether IGFBP5 can modulate the anti-apoptosis function of IGF-1. We found that IGF-1 could block starvation-induced apoptosis of MCF7 cells, which was reversed when IGFBP5 was present in the media (Fig. 3f). Furthermore, IGFBP5 also blocked the pro-survival effect of IGF-1 when cells were treated with cytotoxic agents, including staurosporine, etoposide and doxorubicin (Fig. 3g and Supplementary Fig. 4B,C).

Activation of mTORC1 triggers a number of feedback loops that converge on, and antagonize IGF-1 signalling[9]. We sought to determine the relative contribution of IGFBP5, compared with the known players in these feedback loops. First, we asked the question of how much of the IGF-1-inhibitory activity in $TSC2^{-/-}$ CM could be attributed to IGFBP5. We collected CM from $TSC2^{-/-}$ MEFs with either control or IGFBP5 knockdown, and mixed them with IGF-1, and treated wild-type MEFs. We found that the degree of IGF-1R activation in the recipient cells using the IGFBP5 shRNA $TSC2^{-/-}$ CM is approximately 85% of that using the $TSC2^{+/+}$ CM, indicating that IGFBP5 accounts for a large fraction of the IGF-1-inhibitory activity in $TSC2^{-/-}$ CM (Supplementary Fig. 4D).

We next examined, on the whole-cell level, IGF-1 signalling in $TSC2^{-/-}$ MEFs that were treated with either rapamycin or IGFBP5 shRNA. Both treatments greatly sensitized these cells to IGF-1 stimulation (Supplementary Fig. 4E). We, at the same time, did observe a lower pIGF-1R and pAkt level in IGFBP5 shRNA $TSC2^{-/-}$ MEFs, compared with that in rapamycin-treated GFP shRNA $TSC2^{-/-}$ MEFs (Supplementary Fig. 4E). We then generated $TSC2^{-/-}$ cells with single knockdown of either GRB10 or IGFBP5, as well as cells with GRB10 and IGFBP5 double knockdown (Fig. 4a). Compared with rapamycin treatment, knockdown of either GRB10 or IGFBP5 partially recovered IGF-1-dependent Akt activation. However, $TSC2^{-/-}$ MEFs co-depleted for both GRB10 and IGFBP5 almost completely regained IGF-1 sensitivity (Fig. 4a). Finally, double knockdown of GRB10 and IGFBP5 also markedly accelerates the proliferation of $TSC2^{-/-}$ cells, in response to IGF-1 stimulation (Fig. 4b).

We previously showed that GRB10 is a potential tumour suppressor[8]. As IGFBP5 also inhibits the function of IGF-1 (Fig. 4a), it might be another tumour suppressor downstream of mTORC1. Indeed, at least 20 non-synonymous somatic mutations have been identified for IGFBP5 in cancer (COSMIC database; Supplementary Table 8), including four frameshift (R83fs*65, K135fs*13, R176fs*8 and C192fs*58) and three nonsense mutations (E202*, G223* and W242*; Fig. 4c). We generated mammalian expression constructs (with a carboxy-terminal HA tag) harbouring the individual mutations that have been reported for IGFBP5. We ectopically expressed them in HEK293T cells, collected the corresponding CM, and mixed them with IGF-1. These CM samples were added to wild-type MEFs (Fig. 4d,e). Intriguingly, half of these cancer-associated IGFBP5 mutants completely lost their IGF-1-inhibitory activity, including the above-mentioned truncation mutations, as well as three additional point mutations (G223R, R236H and V244M; Fig. 4d).

Hyperactivation of IGF-1 signalling plays a critical role in establishing a transformed phenotype in a number of malignancies[34]. The development of IGF-1R inhibitors, however, have been largely unsuccessful, in part owing to the lack of a viable approach for patient stratification[35]. We reasoned that the loss of IGFBP5 might drive the survival and proliferation of a cancer cell dependent on IGF-1 signalling. This, in turn, might confer their sensitivity to IGF-1R inhibitors. From the COSMIC database, we identified that NCI-H1435, a non-small-cell lung cancer (NSCLC) cell line, harbours a heterozygous IGFBP5 mutation (E202*) (Fig. 4f). Moreover, the CM from this cell line lacks a detectable signal from IGFBP5 (Supplementary Fig. 5A), indicating the presence of additional misregulation of this protein. Indeed, the proliferation of NCI-H1435 cells was inhibited by various clinically relevant IGF-1R inhibitors, including BMS-536924 and BMS-754807 (ref. 34). Conversely, the growth of IGFBP5-WT NSCLC cell lines, including HCC15, A549, NCI-H1693 and HCC4017, was not affected by IGF-1R inhibitors (Fig. 4g and Supplementary Fig. 5D). Finally, all of these NSCLC cell lines were resistant to a multi-RTK inhibitor, Sunitinib, which, however, is inactive against IGF-1R (ref. 36; Fig. 4g). The proliferation of an *IGFBP5*-mutated leukaemia cell line, Molt-4 (K135fs*13), was also selectively inhibited by IGF-1R inhibitors (Supplementary Fig. 5B). Importantly, the re-expression of IGFBP5 in Molt-4 cells led to their decreased proliferation (Supplementary Fig. 5C).

In summary, our results indicate that mTORC1 positively regulates the expression of IGFBP5 in a HIF1-dependent manner. Once secreted, IGFBP5 functions, in parallel to other intracellular branches of the feedback mechanisms, to block the function of IGF-1 (Fig. 5). IGFBP5 is a potential tumour suppressor, and the proliferation of IGFBP5-mutated cells is sensitive to IGF-1R inhibitors. Finally, our results raise an intriguing hypothesis that IGFBP5 might serve as a 'non-cell autonomous' feedback mechanism for tumours to restrain IGF-1R signalling in adjacent normal cells. In so doing, tumour cells might gain a competitive advantage in growth and proliferation. Whether this mechanism contributes to tumour progression warrants further investigation. □

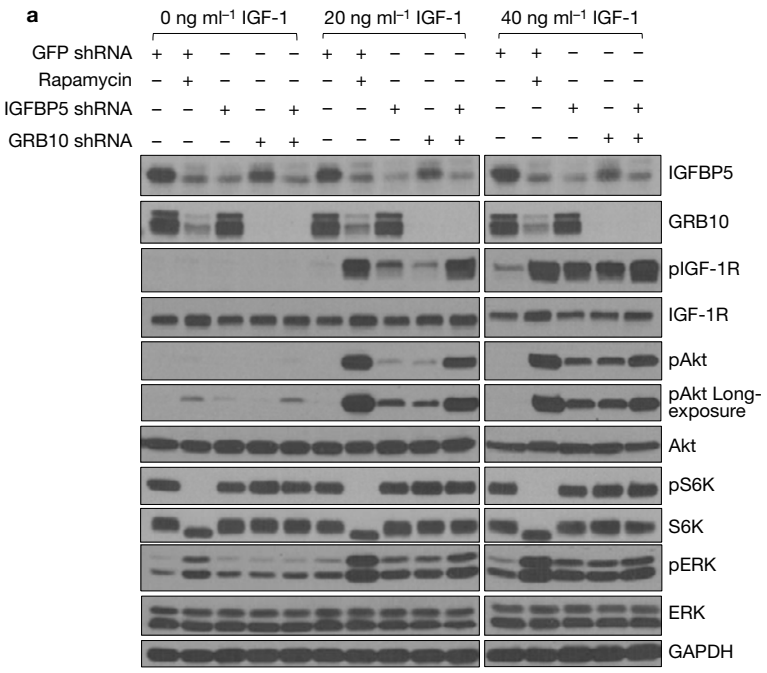

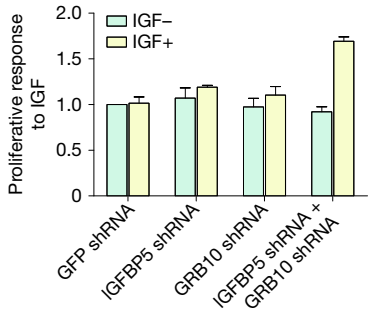

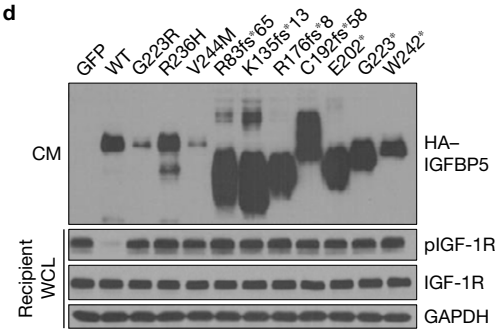

c

COSMIC	Nucleotide	Amino acid	Note	Tissue
Tissue	c.526delC	p.R176fs*8	Frameshift	Pancreas
	c.726G > A	p.W242*	Nonsense	Lung
Cell line	c.247delC	p.R83fs*65	Frameshift	Haematopoietic (GR-ST)
	c.573delC	p.C192fs*58	Frameshift	NS (EN)
	c.402delC	p.K135fs*13	Frameshift	Haematopoietic (MOLT-4)
	c.604G > T	p.E202*	Nonsense	NS (NCI-H1435)
	c.667G > T	p.G223*	Nonsense	NS (SNU-175)

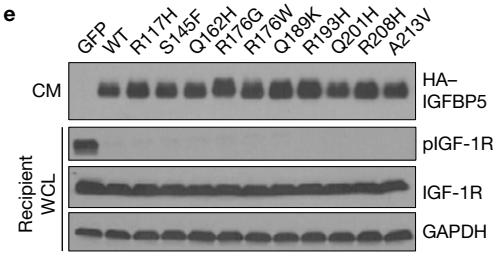

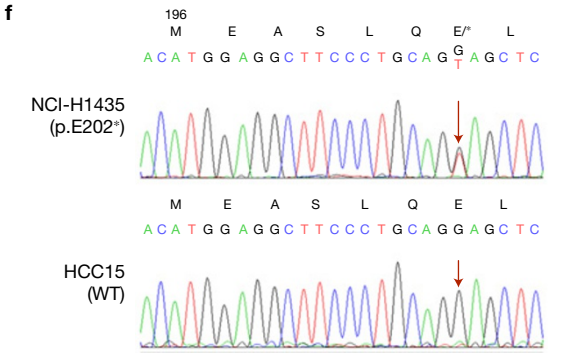

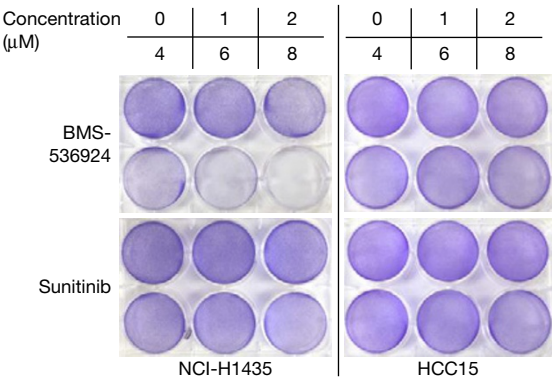

Figure 4 IGFBP5 is a major mediator of mTORC1-dependent feedback inhibition of IGF-1 signalling. (**a**) IGFBP5 and GRB10 together account for a major fraction of the IGF-1-inhibitory activity of mTORC1. We generated *TSC2*$^{-/-}$ MEFs with single IGFBP5 or GRB10 knockdown, as well as IGFBP5+GRB10 double knockdown. Where indicated, cells were also treated with rapamycin (20 nM for 24 h). Cells were stimulated with IGF-1 (at the indicated concentrations). For site-specific phosphorylation, pIGF-1R(Y1135/1136), pAkt(S473), pS6K(T389) and pERK(T202/Y204) levels were analysed. (**b**) GRB10 and IGFBP5 double-knockdown cells show increased proliferative responses in IGF-1-supplemented media. $P < 0.001$ (two-way ANOVA test). $n = 9$ independent biological replicate experiments. Error bars represent s.d. (**c**) Cancer-associated frameshift and nonsense mutations that have been reported for IGFBP5 (data from COSMIC). A complete list of the somatic mutations is shown in Supplementary Table 8. (**d**,**e**) IGFBP5 expression constructs harbouring cancer-associated mutations were transfected into HEK293T cells. Cells were starved, and the corresponding CM was collected, mixed with IGF-1 and incubated with wild-type MEFs (recipient cells). WCL was analysed by immunoblotting experiments using the indicated antibodies. Cancer-associated mutations of IGFBP5 are shown that either disrupt (**d**) or maintain (**e**) its IGF-1-inhibitory activity. For site-specific phosphorylation, pIGF-1R(Y1135/1136) levels were analysed. (**f**) NCI-H1435 cells harbour a heterozygous IGFBP5 mutation (E202*). Genomic fragments in the third exon of IGFBP5 from NCI-H1435 and HCC15 cell lines were amplified with PCR and were sequenced. The red arrows indicate the mutation (G to T) in the NCI-H1435 cell line. HCC15 cells contain wild-type IGFBP5. (**g**) The NCI-H1435 cell line is sensitive to the IGF-1R inhibitor BMS-536924. NCI-H1435 and HCC15 NSCLC cell lines were seeded overnight in 6-well plates at the same density. After 48 h treatment with BMS-536924 or Sunitinib, 6-well plates were fixed with methanol and then were stained with crystal violet. Unprocessed original scans of blots are shown in Supplementary Fig. 6.

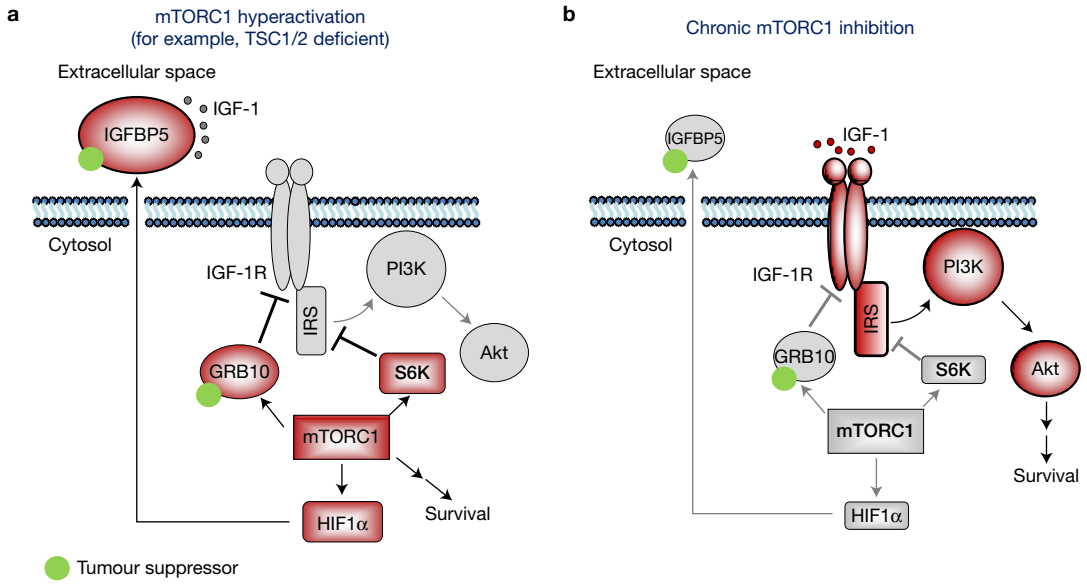

Figure 5 mTORC1 orchestrates feedback inhibition of IGF-1 signalling by promoting HIF1α-dependent expression of IGFBP5. (**a**) IGFBP5 accumulates in the extracellular space, and sequesters IGF-1 from binding to its cognate receptor (IGF-1R). mTORC1 also inhibits IGF-1 signalling by upregulating the expression of GRB10, and downregulating the expression of IRS and IGF-1R. Both GRB10 and IGFBP5 are potential tumour suppressors. (**b**) Conversely, IGF-1R and PI(3)K are activated in mTORC1-suppressed conditions (for example, rapamycin-treated), owing to the relief of mTORC1-mediated feedback inhibition loops. Red and grey indicate proteins that are in the activated and repressed states, respectively.

METHODS

Methods and any associated references are available in the online version of the paper.

Note: Supplementary Information is available in the online version of the paper

ACKNOWLEDGEMENTS

We thank J. Goldstein, J. Blenis, M. White, M. Cobb and B. Tu for critically reviewing the manuscript. We thank J. Minna and D. Kwiatkowski for providing critical reagents, and N. Williams, H. Wang, H. Chen and L. Wu for input and technical guidance. This work was supported in part by grants from the UT Southwestern Endowed Scholar Program (to Y.Y. and R.K.B.), the Cancer Prevention and Research Institute of Texas (CPRIT R1103 to Y.Y. and CPRIT RP130513 to R.K.B.), the Welch Foundation (I-1800 to Y.Y. and I-1568 to R.K.B.), National Institutes of Health (NIH; GM114160 to Y.Y.), American Cancer Society (Research Scholar Grant, RSG-15-062-01-TBE, and Institutional Research Grant, IRG-02-196-07, to Y.Y.), and a Career Award in the Biomedical Sciences from the Burroughs Wellcome Fund (to R.K.B.). Y.Y. is a Virginia Murchison Linthicum Scholar in Medical Research and a CPRIT Scholar in Cancer Research. R.K.B. is the Michael L. Rosenberg Scholar in Medical Research.

AUTHOR CONTRIBUTIONS

Y.Y. conceived the project. M.D., R.K.B. and Y.Y. designed the experiments. M.D. and Y.Y. performed the experiments. R.K.B. provided input on HIF1-related experiments. Y.Y. wrote the manuscript with input from all co-authors.

COMPETING FINANCIAL INTERESTS

The authors declare no competing financial interests.

Published online at http://dx.doi.org/10.1038/ncb3311

Reprints and permissions information is available online at www.nature.com/reprints

1. Dibble, C. C. & Manning, B. D. Signal integration by mTORC1 coordinates nutrient input with biosynthetic output. *Nat. Cell Biol.* **15,** 555–564 (2013).
2. Laplante, M. & Sabatini, D. M. mTOR signalling in growth control and disease. *Cell* **149,** 274–293 (2012).
3. Wouters, B. G. & Koritzinsky, M. Hypoxia signalling through mTOR and the unfolded protein response in cancer. *Nat. Rev. Cancer* **8,** 851–864 (2008).
4. Sancak, Y. *et al.* The Rag GTPases bind raptor and mediate amino acid signalling to mTORC1. *Science* **320,** 1496–1501 (2008).
5. Ma, X. M. & Blenis, J. Molecular mechanisms of mTOR-mediated translational control. *Nat. Rev. Mol. Cell Biol.* **10,** 307–318 (2009).
6. Hsu, P. P. *et al.* The mTOR-regulated phosphoproteome reveals a mechanism of mTORC1-mediated inhibition of growth factor signalling. *Science* **332,** 1317–1322 (2011).
7. Robitaille, A. M. *et al.* Quantitative phosphoproteomics reveal mTORC1 activates *de novo* pyrimidine synthesis. *Science* **339,** 1320–1323 (2013).
8. Yu, Y. *et al.* Phosphoproteomic analysis identifies Grb10 as an mTORC1 substrate that negatively regulates insulin signalling. *Science* **332,** 1322–1326 (2011).
9. Shimobayashi, M. & Hall, M. N. Making new contacts: the mTOR network in metabolism and signalling crosstalk. *Nat. Rev. Mol. Cell Biol.* **15,** 155–162 (2014).
10. Wagle, N. *et al.* Activating mTOR mutations in a patient with an extraordinary response on a phase I trial of everolimus and pazopanib. *Cancer Discov.* **4,** 546–553 (2014).
11. Bissler, J. J. *et al.* Sirolimus for angiomyolipoma in tuberous sclerosis complex or lymphangioleiomyomatosis. *N. Engl. J. Med.* **358,** 140–151 (2008).
12. Wagle, N. *et al.* Response and acquired resistance to everolimus in anaplastic thyroid cancer. *N. Engl. J. Med.* **371,** 1426–1433 (2014).
13. Cloughesy, T. F. *et al.* Antitumor activity of rapamycin in a Phase I trial for patients with recurrent PTEN-deficient glioblastoma. *PLoS Med.* **5,** e8 (2008).
14. Chandarlapaty, S. *et al.* AKT inhibition relieves feedback suppression of receptor tyrosine kinase expression and activity. *Cancer Cell* **19,** 58–71 (2011).
15. Zhang, H. *et al.* PDGFRs are critical for PI3K/Akt activation and negatively regulated by mTOR. *J. Clin. Invest.* **117,** 730–738 (2007).
16. Harrington, L. S. *et al.* The TSC1-2 tumor suppressor controls insulin-PI3K signalling via regulation of IRS proteins. *J. Cell Biol.* **166,** 213–223 (2004).
17. Shah, O. J. & Hunter, T. Turnover of the active fraction of IRS1 involves raptor-mTOR- and S6K1-dependent serine phosphorylation in cell culture models of tuberous sclerosis. *Mol. Cell. Biol.* **26,** 6425–6434 (2006).
18. Liu, P. *et al.* Sin1 phosphorylation impairs mTORC2 complex integrity and inhibits downstream Akt signalling to suppress tumorigenesis. *Nat. Cell Biol.* **15,** 1340–1350 (2013).
19. Yang, G., Murashige, D. S., Humphrey, S. J. & James, D. E. A positive feedback loop between Akt and mTORC2 via SIN1 phosphorylation. *Cell Rep.* **12,** 937–943 (2015).
20. Bhaskar, P. T. *et al.* mTORC1 hyperactivity inhibits serum deprivation-induced apoptosis via increased hexokinase II and GLUT1 expression, sustained Mcl-1 expression, and glycogen synthase kinase 3β inhibition. *Mol. Cell. Biol.* **29,** 5136–5147 (2009).
21. Makridakis, M. & Vlahou, A. Secretome proteomics for discovery of cancer biomarkers. *J. Proteomics* **73,** 2291–2305 (2010).
22. Zhang, Y., Wang, J., Ding, M. & Yu, Y. Site-specific characterization of the Asp- and Glu-ADP-ribosylated proteome. *Nat. Methods* **10,** 981–984 (2013).
23. Cornu, M. *et al.* Hepatic mTORC1 controls locomotor activity, body temperature, and lipid metabolism through FGF21. *Proc. Natl Acad. Sci. USA* **111,** 11592–11599 (2014).

24. Hwa, V., Oh, Y. & Rosenfeld, R. G. The insulin-like growth factor-binding protein (IGFBP) superfamily. *Endocr. Rev.* **20,** 761–787 (1999).
25. Cybulski, N., Polak, P., Auwerx, J., Ruegg, M. A. & Hall, M. N. mTOR complex 2 in adipose tissue negatively controls whole-body growth. *Proc. Natl Acad. Sci. USA* **106,** 9902–9907 (2009).
26. Pearce, L. R. *et al.* Characterization of PF-4708671, a novel and highly specific inhibitor of p70 ribosomal S6 kinase (S6K1). *Biochem. J.* **431,** 245–255 (2010).
27. Duvel, K. *et al.* Activation of a metabolic gene regulatory network downstream of mTOR complex 1. *Mol. Cell* **39,** 171–183 (2010).
28. Li, S., Brown, M. S. & Goldstein, J. L. Bifurcation of insulin signalling pathway in rat liver: mTORC1 required for stimulation of lipogenesis, but not inhibition of gluconeogenesis. *Proc. Natl Acad. Sci. USA* **107,** 3441–3446 (2010).
29. Owen, J. L. *et al.* Insulin stimulation of SREBP-1c processing in transgenic rat hepatocytes requires p70 S6-kinase. *Proc. Natl Acad. Sci. USA* **109,** 16184–16189 (2012).
30. Semenza, G. L. Targeting HIF-1 for cancer therapy. *Nat. Rev. Cancer* **3,** 721–732 (2003).
31. Semenza, G. L. *et al.* Hypoxia response elements in the aldolase A, enolase 1, and lactate dehydrogenase A gene promoters contain essential binding sites for hypoxia-inducible factor 1. *J. Biol. Chem.* **271,** 32529–32537 (1996).
32. Salih, D. A. *et al.* Insulin-like growth factor-binding protein 5 (Igfbp5) compromises survival, growth, muscle development, and fertility in mice. *Proc. Natl Acad. Sci. USA* **101,** 4314–4319 (2004).
33. Miyake, H., Pollak, M. & Gleave, M. E. Castration-induced up-regulation of insulin-like growth factor binding protein-5 potentiates insulin-like growth factor-I activity and accelerates progression to androgen independence in prostate cancer models. *Cancer Res.* **60,** 3058–3064 (2000).
34. Carboni, J. M. *et al.* BMS-754807, a small molecule inhibitor of insulin-like growth factor-1R/IR. *Mol. Cancer Ther.* **8,** 3341–3349 (2009).
35. Chen, H. X. & Sharon, E. IGF-1R as an anti-cancer target-trials and tribulations. *Chin. J. Cancer* **32,** 242–252 (2013).
36. Mendel, D. B. *et al. In vivo* antitumor activity of SU11248, a novel tyrosine kinase inhibitor targeting vascular endothelial growth factor and platelet-derived growth factor receptors: determination of a pharmacokinetic/pharmacodynamic relationship. *Clin. Cancer Res.* **9,** 327–337 (2003).

DOI: 10.1038/ncb3311

METHODS

Cells and reagents. Human embryonic kidney (HEK) 293 cells, RT-4, Molt-4, MCF7 (all from ATCC), NSCLC cells (NCI-H1435, A549, NCI-H1693, HCC4017 and HCC15, which were kind gifts from J. Minna, UT Southwestern Medical Center, USA), and immortalized *TSC2*$^{+/+}$ and *TSC2*$^{-/-}$ mouse embryonic fibroblasts (MEFs; kind gifts from D. Kwiatkowski, Brigham and Women's Hospital, USA) were maintained in Dulbecco's modified Eagle's medium (DMEM) supplemented with 10% fetal bovine serum. Cell lines have been DNA fingerprinted using the PowerPlex 1.2 kit (Promega). All of these cell lines are mycoplasma-free and none of them is in the database for misidentified cell lines. Anti-phospho-Akt (S473) (D9E mAb, cst-4060, 1:1,000 dilution), anti-Akt (C67E7 mAb, cst-4691, 1:1,000 dilution), anti-IGF-1R (D23H3 mAb, cst-9750, 1:1,000 dilution), anti-phospho-IGF-1R (Y1135/Y1136) (19H7 mAb, cst-3024, 1:1,000 dilution), anti-TSC2 (28A7 mAb, cst-3635, 1:1,000 dilution), anti-S6K (cst-9202, 1:1,000 dilution), anti-phospho-S6K (T389) (cst-9205, 1:1,000 dilution), anti-phospho-ERK1/2 antibody (D13.14.4E mAb, cst-4370, 1:1,000 dilution), anti-PARP1 (46D11 mAb, cst-9532, 1:1,000 dilution), and anti-phospho-ribosomal protein S6 (S235/S236) (D68F8, cst-5364, 1:1,000 dilution) were obtained from Cell Signaling Technology. The rabbit anti-HIF1α antibody (A300-286A, 1:1,000 dilution) was purchased from Bethyl Laboratories, LLC. Anti-IGFBP5 (H-100, sc-13093, 1:500 dilution) and anti-GRB10 (K-20, sc-1026, 1:1,000 dilution) antibodies were obtained from Santa Cruz Biotechnology. Insulin, IGF-1, epidermal growth factor (EGF), platelet-derived growth factor (PDGF), hepatocyte growth factor (HGF) and Polybrene were purchased from Sigma. Lipofectamine 2000 was purchased from Invitrogen. LDH cytotoxicity assay kit was obtained from Pierce (Life technologies). Sequences for primers used in quantitative RT–PCR, luciferase reporter assays and ChIP assays are shown in Supplementary Tables 1–3.

SILAC cell culture. *TSC2*$^{-/-}$ MEFs were grown in light ($[^{12}C_6^{14}N_2]$Lys, $[^{12}C_6^{14}N_4]$Arg) and heavy ($[^{13}C_6^{15}N_2]$Lys, $[^{13}C_6^{15}N_4]$Arg) DMEM (Cambridge Isotope Labs), respectively. Both light and heavy DMEM were supplemented with 10% dialysed FBS (Invitrogen). Dialysed FBS was used to avoid the introduction of light amino acids that are naturally present in the serum. Cells were grown in the corresponding media for 7 passages, at which point an incorporation check was performed. Specifically, heavy cells were isolated, lysed and digested overnight with sequencing-grade trypsin (Promega) at a 1:100 (enzyme/substrate) ratio (see the next section for detailed description of the digestion conditions). Peptides were desalted using SepPak C18 columns (Waters) according to the manufacturer's instructions, and were subsequently analysed by LC–MS/MS experiments on an LTQ Velos Pro Orbitrap mass spectrometer (Thermo). The incorporation rate of heavy amino acids ($[^{13}C_6^{15}N_2]$Lys, $[^{13}C_6^{15}N_4]$Arg) was found to be around 97% under these conditions.

Sample preparation for mass spectrometric analysis. SILAC-labelled *TSC2*$^{-/-}$ MEFs were serum-deprived for 24 h, during which cells cultured in light media were treated with 20 nM rapamycin. Conditioned medium (CM) was collected, which was centrifuged at 1,500 r.p.m. (239*g*) for 15 min to remove residual cells. The CM samples were further filtered through 0.45 μm filters.

The light and heavy CM were combined at a 1:1 ratio (normalized by cell lysates), and then concentrated by a Centricon ultrafiltration unit (Millipore, MWCO = 5,000 Da). Proteins were extracted by methanol–chloroform precipitation, and were then solubilized in 8 M urea. Cysteines were reduced by 2 mM dithiothreitol, and were then alkylated by adding iodoacetamide to a final concentration of 50 mM, followed by incubation in the dark for 20 min. The lysates were diluted to a final concentration of 2 M urea by addition of 100 mM ammonium bicarbonate (pH 7.8) and were digested overnight with sequencing-grade trypsin (Promega) at a 1:100 (enzyme/substrate) ratio. Digestion was quenched by addition of trifluoroacetic acid to a final concentration of 0.1% and precipitates were removed by centrifugation at 4,000 r.p.m. (1,699*g*) for 30 min. Peptides were desalted using SepPak C18 columns (Waters) according to the manufacturer's instructions.

Peptides were fractionated by using an off-line two-dimensional SCX-RP-HPLC (strong-cation-exchange reversed-phase HPLC) protocol[37]. Briefly, lyophilized peptides were resuspended in 500 μl SCX buffer A (5 mM KH_2PO_4, pH 2.65, 30% acetonitrile) and injected onto a SCX column (polysulphoethyl aspartamide, 4.6 mm × 200 mm, 5 μM particle size, 200 Å pore size, PolyLC). A gradient was developed over 35 min ranging from 0 to 21% buffer B (5 mM KH_2PO_4, pH 2.65, 30% acetonitrile, 350 mM KCl) at a flow rate of 1 ml min^{-1}. Twelve fractions were collected and lyophilized. Peptides were then desalted using SepPak C18 columns and lyophilized. In the second dimension, peptides were separated on a 75 μm × 15 cm in-house packed RP column (Maccel 200-3-C18AQ, 3 μm, 200 Å) using a gradient developed over 90 min ranging from 0% to 37% buffer B (97% acetonitrile, 0.1% formic acid). Peptides were directly introduced into the mass spectrometer using a hand-pulled emitter.

Mass spectrometry analysis and data processing. The SILAC sample was analysed by LC–MS/MS experiments on an LTQ Velos Pro Orbitrap mass spectrometer (Thermo) using a top-20 CID (collision-induced dissociation) method[38]. MS/MS spectra were searched against a composite database of the mouse IPI protein database (Version 3.60) and its reversed complement using the Sequest algorithm. Search parameters allowed for a static modification of 57.02146 Da for cysteine and a dynamic modification of oxidation (15.99491 Da) on methionine, stable isotope (10.00827 Da) and (8.01420 Da) on arginine and lysine, respectively. Search results were filtered to include <1% matches to the reverse database by the linear discriminator function using parameters including Xcorr, dCN, missed cleavage, charge state (exclude 1+ peptides), mass accuracy, all heavy or light Lys and Arg, peptide length and fraction of ions matched to MS/MS spectra[39]. Peptide quantification was performed by using the CoreQuant algorithm[39]. As serum proteins are always light (residual proteins from FBS), we further removed the peptides in which only the light ion is present (the signal-to-noise ratio of the heavy peptide equals zero). A step-by-step protocol of the mass spectrometry analysis can be found at Nature Protocol Exchange[40].

From this SILAC CM sample, we identified and quantified a total of 61,920 peptides from 3,099 proteins (peptide false discovery rate = 0.27%; Fig. 1d and Supplementary Tables 4–7). We sorted the proteins on the basis of their number of identified peptides. The top five proteins are fibronectin, plectin-1, collagen alpha-2(I) chain, filamin-A and collagen alpha-1(I) chain, all of which are known secreted or membrane-bound proteins. These proteins were confidently identified, with sequence coverage of 64.8%, 52.8%, 87.7%, 66.1% and 81.8%, respectively. The list also contains many secreted proteins that are known to be expressed at low abundances, including chemokines (CCL2, CCL7, CCL9, CXCL1, CXCL5 and CXCL16) and growth factors (TGFB2, TGFB3, HDGF and CTGF). The identification of these extracellular signalling molecules demonstrates the excellent sensitivity of our MS method.

We also performed a biological replicate SILAC experiment (SILAC experiment no. 2) with switched isotope labels (that is, heavy cells treated with rapamycin). In this experiment, we identified 3,927 proteins from the CM of *TSC2*$^{-/-}$ MEFs. In total, we identified 4,195 unique proteins from these two sets of SILAC CM samples. Cross-reference analysis indicates that 2,825 proteins were commonly identified between the two SILAC experiments, yielding a reproducibility of 71.9% (Supplementary Fig. 1D).

As rapamycin treatment abrogated the expression of the IGF-1-inhibitory protein (Fig. 1a), we focused our follow-up analysis on proteins whose abundances decreased as a result of mTORC1 inhibition. Gene ontology (cellular compartment) analysis of these proteins showed that they were highly enriched for extracellular matrix proteins ($P = 6.5 \times 10^{-10}$; Supplementary Fig. 2A). Furthermore, we submitted this group of proteins, and compared them with the human Plasma Proteome Database[41]. The results show that of the 355 proteins, 301 (84.8%) have been found previously in plasma, again highlighting that this list is enriched with extracellular proteins.

mTOR inhibitor treatment. Inhibition of mTORC1 in *TSC2*$^{-/-}$ MEFs by either rapamycin or mTOR kinase inhibitors (Ku0063794 and NVP-BEZ235[42]) resulted in a marked decrease of IGFBP5 (Fig. 1f–h). In contrast, treatment of these cells with an S6K inhibitor, PF-4708671 (ref. 26), had no effect on IGFBP5 levels (Fig. 1h). These results indicate that mTORC1 itself, rather than S6K, regulates the expression of IGFBP5. We also show that mTORC1 regulates the expression of IGFBP5 in other cell lines. Specifically, rapamycin treatment of RT-4 cells (a *TSC1*-deficient bladder cancer cell line[43]) also resulted in marked reduction of the abundance of secreted IGFBP5 (Supplementary Fig. 1H). To investigate whether mTORC1 is involved in regulating the expression of IGFBP5 in *TSC1/2*-proficient cells, we starved MCF7 cells and then stimulated them with insulin. We found that this treatment led to robust accumulation of IGFBP5 in CM, which was strongly suppressed when cells were concurrently treated with rapamycin (Supplementary Fig. 1I).

Plasmids. The cDNA for human and mouse IGFBP5 was obtained from Invitrogen, amplified by PCR, and cloned into a pKH3 vector. Cancer-associated IGFBP5 mutants were generated using the QuickChange site-directed mutagenesis kit (Stratagene). Lentiviral plasmids (Δ8.9 and VSVG) were kind gifts from A. Kung (Dana Farber Cancer Institute, USA) and D. Baltimore (California Institute of Technology, USA).

Mammalian lentiviral shRNAs. Lentiviral short hairpin RNA (shRNA) in pLKO.1 expression vectors were obtained from Sigma. The shRNA sequences are listed in Supplementary Table 9. To generate the lentiviruses, shRNA plasmids were co-transfected into HEK293TD cells along with packaging (Δ8.9) and envelope (VSVG) expression plasmids using Lipofectamine 2000 (Invitrogen). Two days after transfection, viral supernatants were collected and filtered. Recipient cells were infected in the presence of a serum-containing medium supplemented with

8 μg ml^{-1} Polybrene. Following infection for 36 h, cells were treated with 2.0 μg ml^{-1} puromycin (Sigma) and cell lines that stably expressed the shRNAs were selected. Knockdown efficiencies were examined by immunoblot assay using antibodies against the target protein.

Depletion of IGFBP5 sensitizes *TSC2*$^{-/-}$ MEFs to IGF-1 stimulation. Specifically, *TSC2*$^{-/-}$ MEFs exhibited a profound 'IGF-1-resistant' state, as indicated by the lack of IGF-1R activation, on IGF-1 stimulation (Fig. 3b). Intriguingly, RNAi-mediated knockdown of IGFBP5 in *TSC2*$^{-/-}$ MEFs greatly sensitizes them to IGF-1 stimulation (Fig. 3b). Using a quantitative ELISA approach, we determined the concentration of IGFBP5 in CM of *TSC2*$^{-/-}$ MEFs (starved for 24 h at 90% confluency) to be about 300 ng ml^{-1}. For 40 ng ml^{-1} of IGF-1, this translates into a molar ratio between IGFBP5 and IGF-1 of ~4:1. We have also found this medium is able to inhibit up to 80 ng ml^{-1} of IGF-1 (2:1 between IGFBP5 and IGF-1; not shown). These IGFBP5 concentrations and IGFBP5/IGF-1 ratios are in fact close to those in serum samples from rats and humans[44,45].

Immunoblot analysis. For immunoblot analysis, the cells were extracted in lysis buffer (20 mM HEPES pH 7.5, 1% Triton X-100, 150 mM NaCl, 10 mM EDTA, 1 mM EGTA, 1 mM sodium orthovanadate, 1 mM NaF, 2 mM phenylmethylsulphonyl fluoride, 2 mg ml^{-1} aprotinin, 2 mg ml^{-1} leupeptin, and 1 mg ml^{-1} pepstatin), and extracts were mixed with the 5× reducing buffer (60 mM Tris-HCl, pH 6.8, 25% glycerol, 2% SDS, 14.4 mM 2-mercaptoethanol, 0.1% bromophenol blue). Samples were boiled for 5 min and subject to electrophoresis using the standard SDS–PAGE method. Proteins were then transferred to a nitrocellulose membrane (Whatman). The membranes were blocked with a TBST buffer (25 mM Tris-HCl, pH 7.5, 150 mM NaCl, 0.05% Tween 20) containing 3% non-fat dried milk, and probed overnight with primary antibodies (1:1,000 dilution) at 4 °C and for 1 h at room temperature with peroxidase-conjugated secondary antibodies. Blots were developed using enhanced chemiluminescence, exposed on autoradiograph film and developed using standard methods. Western blot images were quantified by using the software package ImageJ.

Quantitative RT–PCR analysis. Total RNA from *TSC2*$^{-/-}$, *TSC2*$^{+/+}$ MEFs or RT-4 cells was extracted with the RNeasy Mini Kit (Qiagen) from three independently collected cells. Two micrograms of total RNA was used in each first-strand cDNA synthesis reaction with SuperScript III Reverse Transcriptase (Invitrogen). To perform quantitative real-time PCR, Power SYBR Green Master Mix (Applied Biosystems) was used together with a 7900 HT detection system. Data were analysed using the comparative Ct method and the expression level of each gene was normalized to the *ACTB* gene. To perform semiquantitative PCR, Taq DNA polymerase (Invitrogen) was used. The primers used to amplify *ACTB*, *IGFBP5*, *VEGF*, *PGK1* and *GAPDH* are listed in Supplementary Table 1.

***In vitro* co-culture experiment.** Lentiviruses carrying green fluorescent protein (pLenti6–EGFP) or red fluorescent protein (pLJM1–DsRed) were used to infect *TSC2*$^{-/-}$ MEFs and MCF7 cells, respectively. *TSC2*$^{-/-}$ cells were further infected by pLKO.1–Scramble-shRNA or pLKO.1–IGFBP5-shRNA lentivirus. MCF7 cells were then grown with *TSC2*$^{-/-}$ MEFs with either Scramble shRNA or IGFBP5 shRNA for 48 h in DMEM supplemented with 40 ng ml^{-1} IGF-1. Photos of the cells were analysed with ImageJ software to count the green or red cell numbers.

Luciferase reporter assay. The pGL4.42 (luc2P/HRE/Hygro) vector (Promega) containing four copies of HRE was used as the positive control in the luciferase reporter assay. To explore the potential HRE sites in the *IGFBP5* gene, fragments of *IGFBP5* that are upstream and downstream of the genomic transcription start site were amplified and were used to substitute the HRE site between the XhoI and KpnI sites in the pGL4.42 vector. Four reporter vectors were generated with this strategy, pGL4.P1 (P1, −1.5 kb ~ −50 bp), pGL4.P2 (P2, −0.6 kb ~ −50 bp), pGL4.P3 (P3, +0.1 kb ~ +0.9 kb), pGL4.P4 (P4, +2.9 kb ~ +3.2 kb). The sequences of the primers and the relative distance from the IGFBP5 transcription start site are listed in Supplementary Table 2. To perform the luciferase reporter assay, these pGL4 reporter vectors were co-transfected with pcDNA3.1-HIF1α or pcDNA3.1 empty vector into HEK293T cells. The pGL4–hRluc expressing the *Renilla reniformis* luciferase under the TK promoter was used as the internal control in each experiment. Forty-eight hours after transfection, cells cultured in either normoxic or hypoxic (1% O_2) conditions were collected and were used to determine the luciferase activity using the protocol from Promega. Experiments were performed in triplicate.

Chromatin immunoprecipitation (ChIP). Two 15 cm plates of RT4 cells (70% confluency) were used for the ChIP experiment after overnight incubation in hypoxic (1% O_2) conditions. The medium was removed and 1% paraformaldehyde (Thermo Fisher Scientific) in PBS was added into the culture plate. The plates were slowly shaken for 10 min at room temperature, and the crosslinking reagent was quenched with 1 ml 2.5 M glycine. The crosslinked cells were collected with cell lysis buffer (10 mM HEPES, pH 8.0, 85 mM KCl, 0.5% NP-40). Crude nuclear pellets were treated with 50 U MNase for 1 h on ice. EDTA was added to a final concentration of 50 mM to inactivate MNase. After centrifugation, nuclear extracts (dissolved in the nuclei extraction buffer, 50 mM Tris-HCl, pH 8.0, 10 mM EDTA, 1% SDS) were sonicated on ice until the size of the fragmented DNA reached between 300~1,000 bp. Fragmented chromatin was diluted with 10 volumes of dilution buffer (50 mM Tris-HCl, pH 8.0, 10 mM EDTA) for the ChIP experiments. ChIP was performed using an anti-HIF1α (Bethyl Laboratories) antibody and normal IgG (Santa Cruz Biotechnology) was used as the control. The genomic DNA recovered from ChIP was analysed by real-time qPCR using primers specific to the −1.5 kb, −0.5 kb, and +3.0 kb region of the IGFBP5 promoter. Experiments were performed in triplicate.

Statistics and repeatability of experiments. All immunoblotting experiments were independently repeated at least three times. Quantification and statistical data processing were performed by using ImageJ and GraphPad Prism, respectively. The results for significance tests are included in the legend of each figure. The qPCR experiments in Fig. 2g,h were performed with RNA prepared from three independent biological replicate experiments. The luciferase reporter assays in Fig. 2i,k were repeated three times with independent transfection. The ChIP assay in Fig. 2j was independently repeated three times.

Accession links. The proteomic data can be downloaded from the Chorus database using the following links: https://chorusproject.org/anonymous/download/experiment/4a5364d20d784bad95d69862e4ba23fa and https://chorusproject.org/anonymous/download/experiment/52afeb2040a5472ea543531f751d9fa4.

37. Villen, J., Beausoleil, S. A., Gerber, S. A. & Gygi, S. P. Large-scale phosphorylation analysis of mouse liver. *Proc. Natl Acad. Sci. USA* **104,** 1488–1493 (2007).
38. Olsen, J. V. *et al.* A dual pressure linear ion trap Orbitrap instrument with very high sequencing speed. *Mol. Cell. Proteomics* **8,** 2759–2769 (2009).
39. Huttlin, E. L. *et al.* A tissue-specific atlas of mouse protein phosphorylation and expression. *Cell* **143,** 1174–1189 (2010).
40. Ding, M., Bruick, R. & Yu, Y. Secreted IGFBP5 mediates mTORC-1-dependent feedback inhibition of IGF1 signaling. *Protocol Exchange* http://dx.doi.org/10.1038/protex.2015.124 (2015).
41. Nanjappa, V. *et al.* Plasma Proteome Database as a resource for proteomics research: 2014 update. *Nucleic Acids Res.* **42,** D959–D965 (2014).
42. Maira, S. M. *et al.* Identification and characterization of NVP-BEZ235, a new orally available dual phosphatidylinositol 3-kinase/mammalian target of rapamycin inhibitor with potent *in vivo* antitumor activity. *Mol. Cancer Ther.* **7,** 1851–1863 (2008).
43. Guo, Y. *et al.* TSC1 involvement in bladder cancer: diverse effects and therapeutic implications. *J. Pathol.* **230,** 17–27 (2013).
44. Jehle, P. M., Jehle, D. R., Mohan, S. & Bohm, B. O. Serum levels of insulin-like growth factor system components and relationship to bone metabolism in Type 1 and Type 2 diabetes mellitus patients. *J. Endocrinol.* **159,** 297–306 (1998).
45. Kong, S. E., Baxter, R. C. & Delhanty, P. J. Age-dependent regulation of the acid-labile subunit in response to fasting-refeeding in rats. *Endocrinology* **143,** 4505–4512 (2002).

nature cell biology

DOI: 10.1038/ncb3311

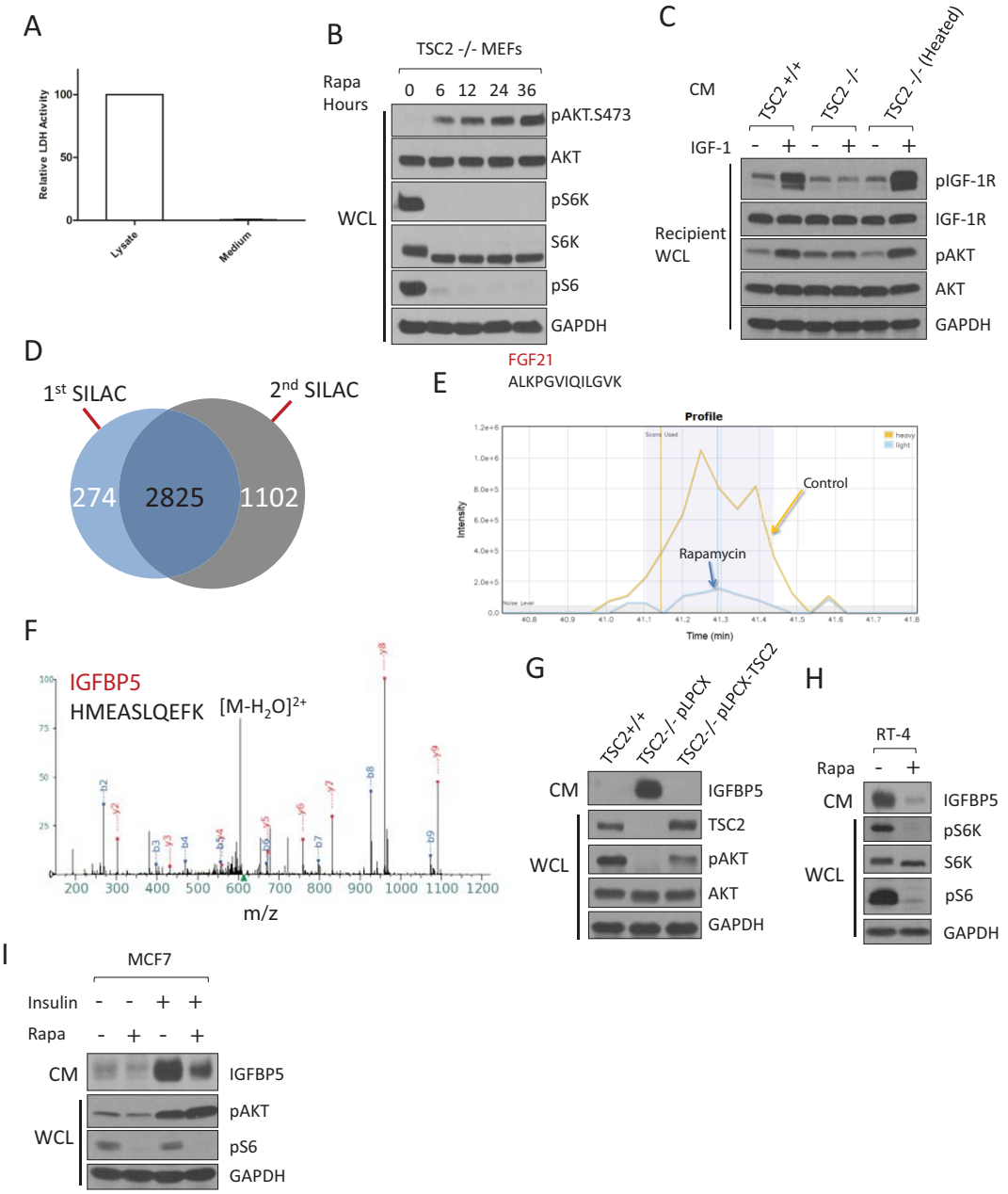

Supplementary Figure 1 (A) LDH activity in the whole cell lysates and conditioned media from *TSC2-/-* MEFs was quantified using a coupled enzymatic colorimetric assay. LDH is a cytosolic enzyme that is found in nearly all living cells. (B) Chronic rapamcyin treatment (20 nM) of *TSC2-/-* MEFs led to Akt activation. For site-specific phosphorylation, pAkt(S473), pS6K(T389) and pS6(S235/236) levels were analyzed. (C) Heat-inactivated CM from *TSC2-/-* MEFs lost its ability to inhibit IGF-1 signaling. CM was collected from *TSC2-/-* MEFs and was heated at 95 ºC for 5 mins. CM was then mixed with IGF-1 (40 ng/ml) and added to wt MEFs, the WCL of which were analyzed. For site-specific phosphorylation, pIGF-1R(Y1135/1136) and pAkt(S473) levels were analyzed. (D) Proteins identified from the two SILAC experiments. (E) Identification of FGF21 as a downstream target of mTORC1 in the extracellular space. Extracted ion chromatogram is shown for the corresponding light (rapamycin-treated, blue) and heavy (control, yellow) ions of a peptide (ALKPGVIQILGVK) from FGF21. This peptide showed a dramatic decrease after rapamycin treatment. (F) Identification of an IGFBP5 peptide (HMEASLQEFK). The MS2 spectrum from which the peptide was identified (matched *b*- and *y*- ions are highlighted in blue and red, respectively) is shown. (G) Re-introducing *TSC2* into *TSC2-/-* MEFs led to dramatic downregulation of IGFBP5 in CM. For site-specific phosphorylation, pAkt(S473) levels were analyzed. (H) Rapamycin treatment also downregulated the expression of IGFBP5 in RT-4 cells. RT-4 cells were starved for 24 hrs, during which cells were treated with 20 nM rapamycin. For site-specific phosphorylation, pS6K(T389) and pS6(S235/236) levels were analyzed. (I) Insulin stimulation of MCF7 cells resulted in the accumulation of IGFBP5 in CM, which was blocked by concurrent rapamycin treatment. Cells were starved for 12 hrs, and were then treated with insulin (100 nM) for 12 hrs, in the absence or presence of rapamycin (20 nM). For site-specific phosphorylation, pAkt(S473) and pS6(S235/236) levels were analyzed.

A

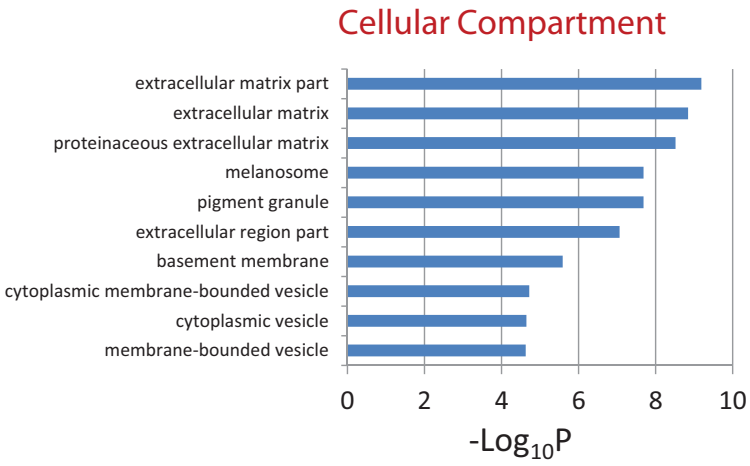

B

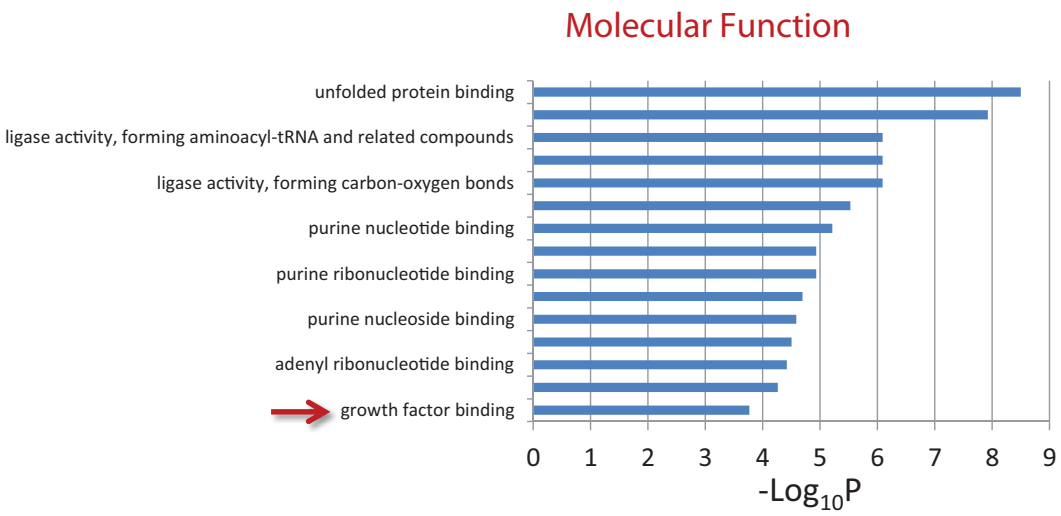

Supplementary Figure 2 Gene ontology analysis of the rapamycin-sensitive proteins (abundances decreased by at least 32-fold after rapamycin treatment). (A) Cellular compartment analysis. (B) Molecular function analysis. For clear presentation, only results from SILAC experiment #1 were considered.

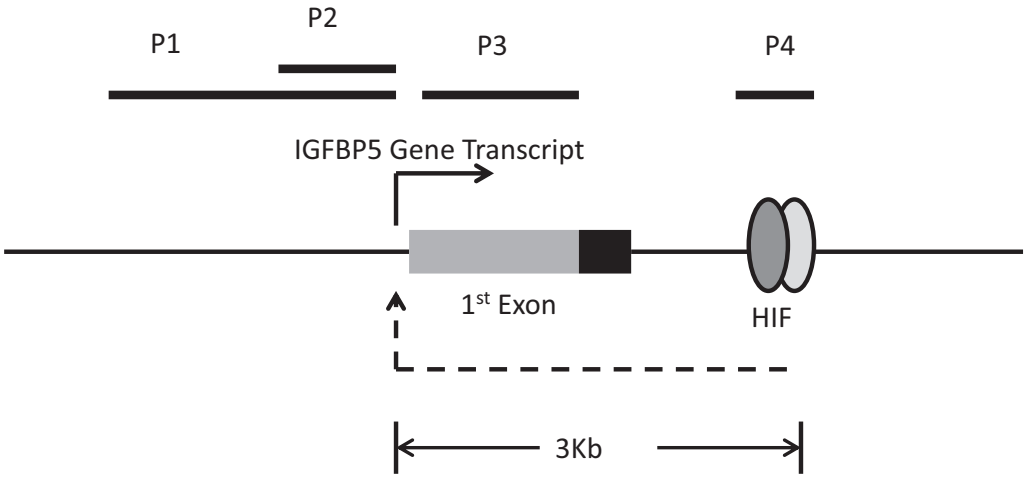

IGFBP5 +2.9 ---- +3.1 Kb sequence

CTTCATCTTGGGGGATGTGGATTTGGAAAAGCCTAGCGGAGAAGGAA
AACATTAATTGATTTCCCGGCTTGGGAGCCACCGCCCTGGGTAACAATC
CAGTCACACCGAAAGAACGTAAGGTGTCACTCAGCCGCATCCTGGCTC
CACTTATTATTTACCAAGCGTGTAGTGTGATGTGGCTAGTGTGAAGGG
TGTACACGCAGAGCGCACGCGCGCAATTGCTAGGCGAGCAC
GGAGGGCGCATCACACACACACACACACACACACACACACACACACA
CACACGACACTTCAGTCC

HRE1 HRE2 HRE3 HRE4 HRE5

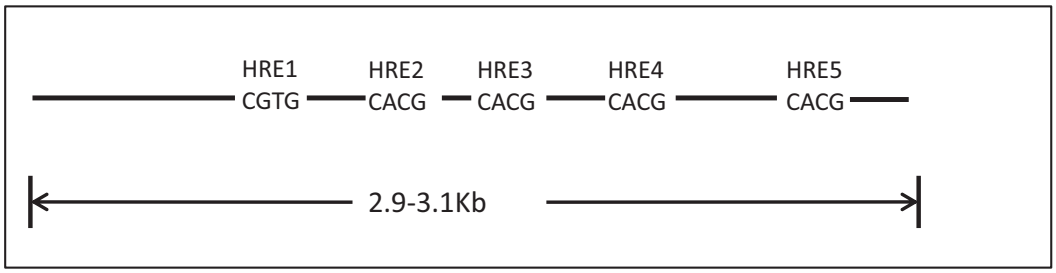

Supplementary Figure 3 A schematic indicating the possible model of HIF1-regulated expression of *IGFBP5*. The design of various primers (P1-P4) capturing potential HIF1α binding sites on *IGFBP5* is shown.

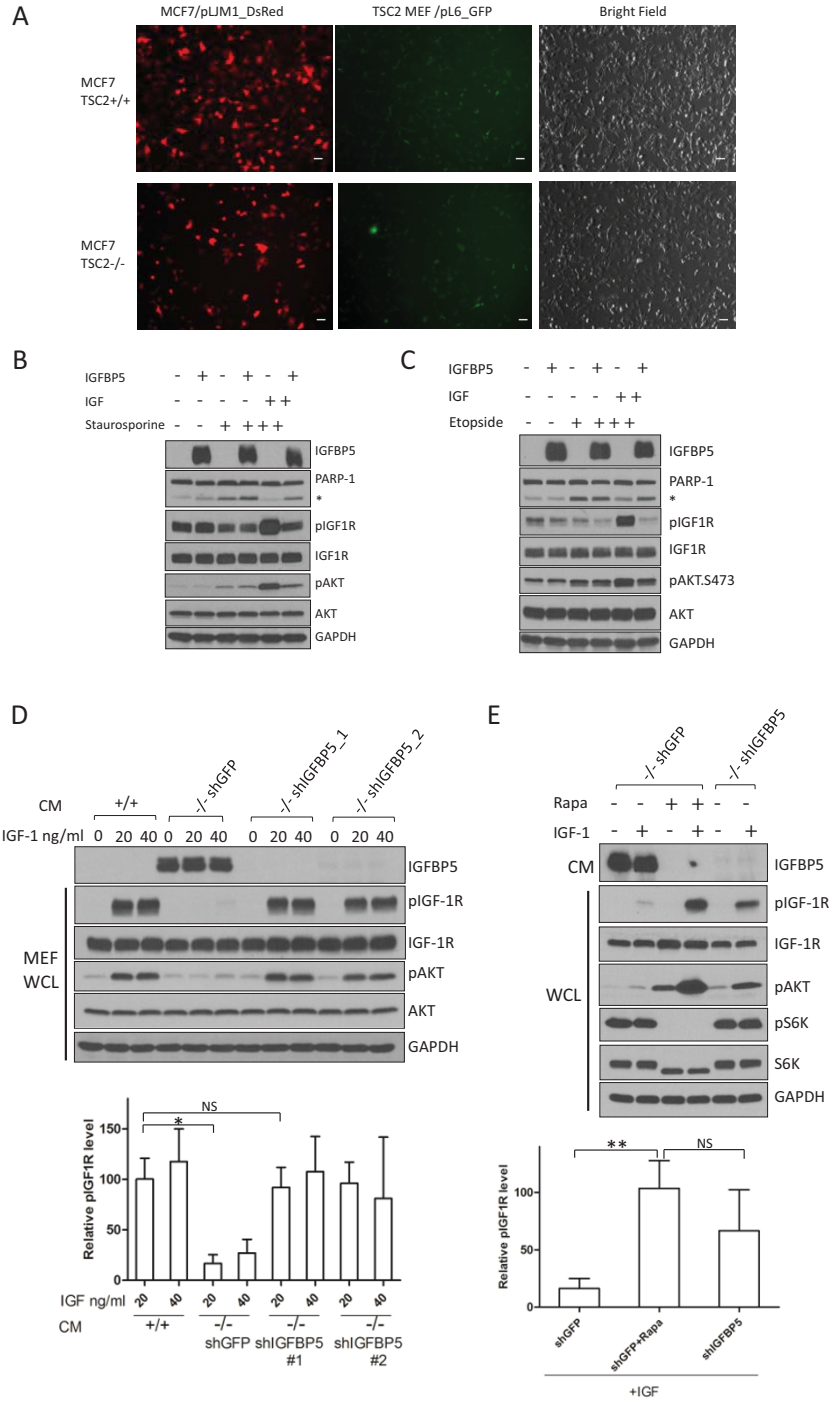

Supplementary Figure 4 (A) Proteins secreted from *TSC2-/-* MEFs inhibits the growth of MCF7 cells in a co-culture system. MCF7 cells were labeled with red florescent protein (DsRed), and were grown with GFP-labeled either *TSC2+/+* or *TSC2-/-* MEFs. Cells were grown in DMEM supplemented with IGF-1. Scale bars, 40 μm. IGF-1 protects cells from staurosporine, (B), or etoposide (C)-induced apoptosis. This effect was abolished when IGFBP5 was co-added to the culture media. The asterisk indicates cleaved PARP1. For site-specific phosphorylation, pIGF-1R(Y1135/1136) and pAkt(S473) levels were analyzed. (D) IGFBP5 accounts for a major fraction of the IGF-1-inhibitory activity in CM from *TSC2-/-* MEFs. CM from *TSC2+/+*, shGFP *TSC2-/-* or shIGFBP5 *TSC2-/-* cells were mixed with IGF-1, and were added to recipient cells (wild type MEFs). WCL were analyzed by immunoblotting experiments using the indicated antibodies. The results were quantified using ImageJ. For site-specific phosphorylation, pIGF-1R(Y1135/1136) and pAkt(S473) levels were analyzed. $^{*}P < 0.05$ (two-tailed Student *t*-test), NS=Not significant, n = 3 independent biological replicate experiments. Error bars represent s.d. (E) IGFBP5 mediates the mTORC1-dependent IGF-1-inhibitory activity in *TSC2-/-* MEFs. RNAi was used to knock down IGFBP5 in *TSC2-/-* MEFs. Where indicated, control knock down cells (shGFP *TSC2-/-* MEFs) were treated with rapamycin (20 nM for 24 hrs). The results were quantified using ImageJ. For site-specific phosphorylation, pIGF-1R(Y1135/1136), pAkt(S473) and pS6K(T389) levels were analyzed. pIGF-1R levels were normalized using total IGF-1R levels (note the rapamycin treatment increases total IGF1-R levels). $^{**}P < 0.01$ (two-tailed Student *t*-test), NS=Not significant. n = 4 independent biological replicate experiments. Error bars represent s.d.

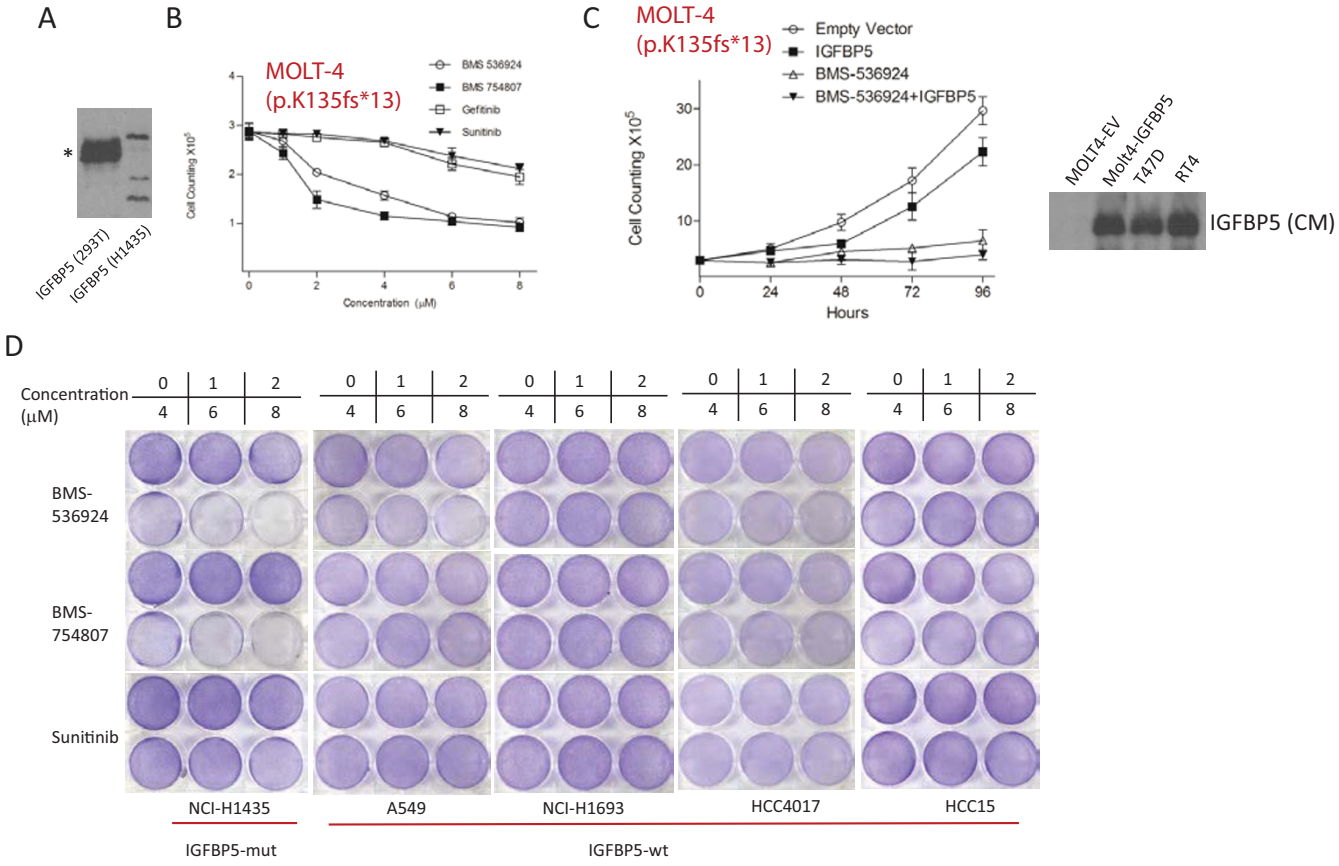

Supplementary Figure 5 (A) CM from NCI-H1435 cells does not contain detectable IGFBP5 signals. CM from HEK293T cells that ectopically express IGFBP5 is used as the control. (B) Molt-4 cells (an acute lymphoblastic leukemia cell line that harbors a K135fs*13 mutation of the *IGFBP5* gene) is more sensitive to IGF-1R inhibitors (BMS-536924 and BMS-754807), compared to Gefitinib and Sunitinib (48 hours treatment). P <0.001 (two-way ANOVA test). n=9 independent biological replicate experiments. Error bars represent s.d. (C) The expression of wt-*IGFBP5* in Molt-4 cells (to a level similar to that in *IGFBP5*-wt cells, e.g. T47D and RT-4) leads to reduced proliferation of these cells (grown in DMEM supplemented with 10% FBS). BMS-536924 treatment (500 nM) was used as the control. (D) The proliferation of *IGFBP5*-mutated (NCI-H1435), but not *IGFBP5*-wt (A549, NCI-H1693, HCC4017 and HCC15) NSCLC cells is sensitive to IGF-1R inhibitors (BMS-536924 and BMS-754807). None of these cells were sensitive to Sunitinib, a multi-RTK inhibitor, which, however, does not block IGF-1R.

Figure1 1.A

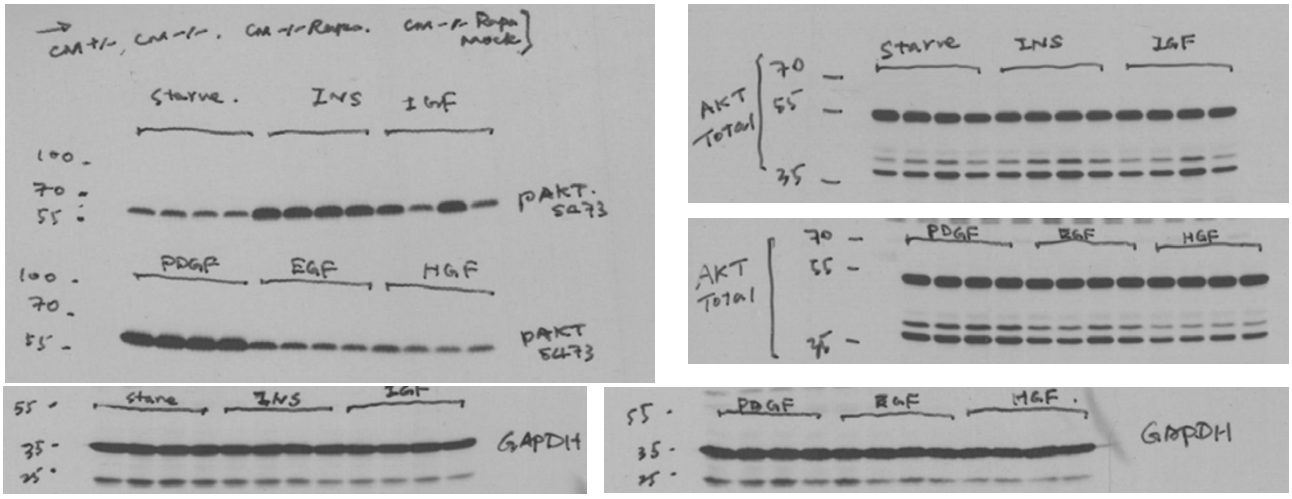

1.B

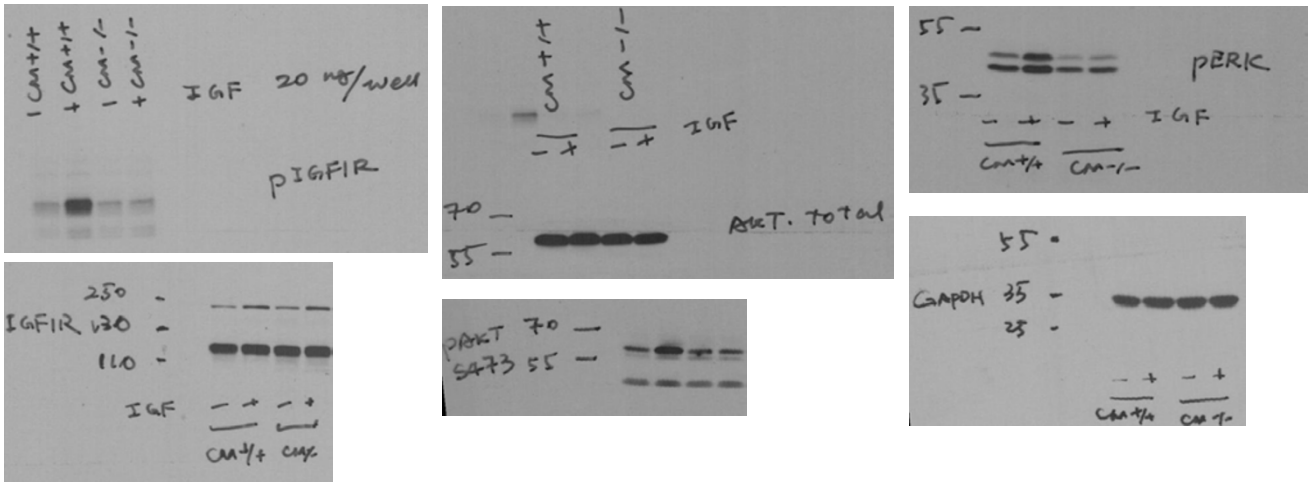

Supplementary Figure 6 Raw, uncropped images of the immunoblotting results.

1.D

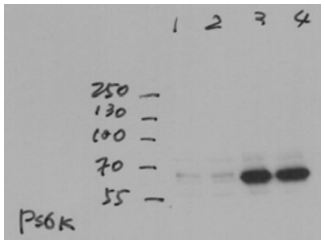

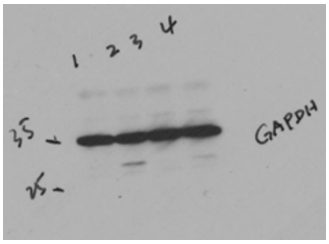

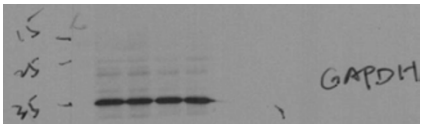

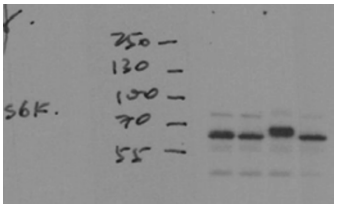

1.F

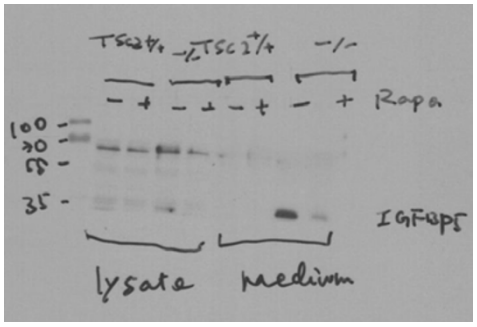

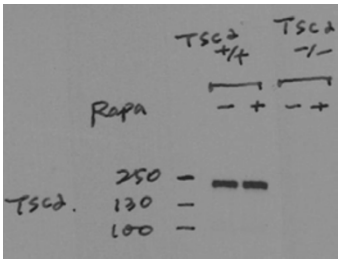

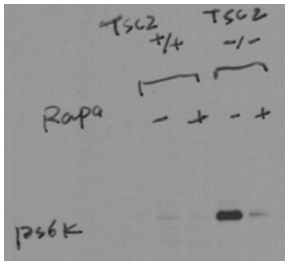

1.G

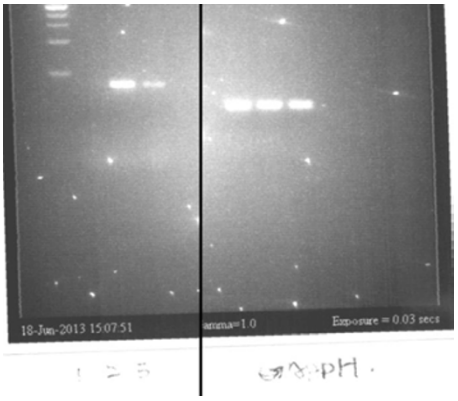

Supplementary Figure 6 continued

1.H

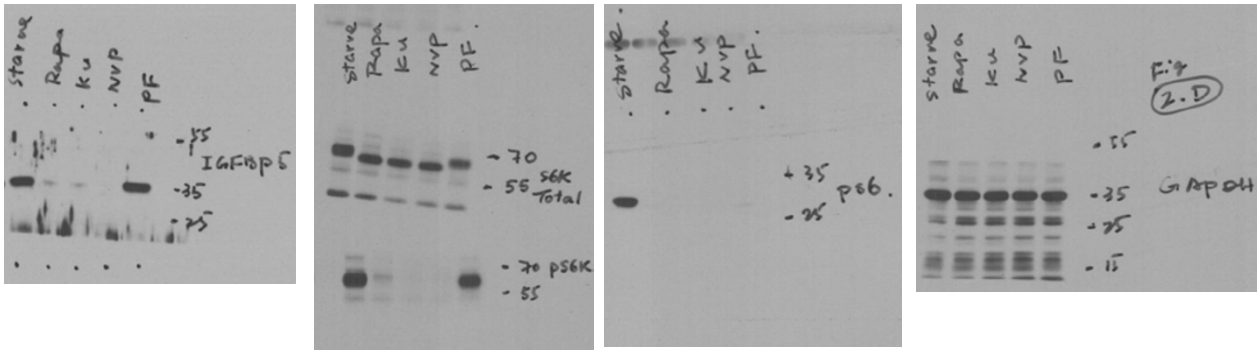

Figure2 2.A 2.B

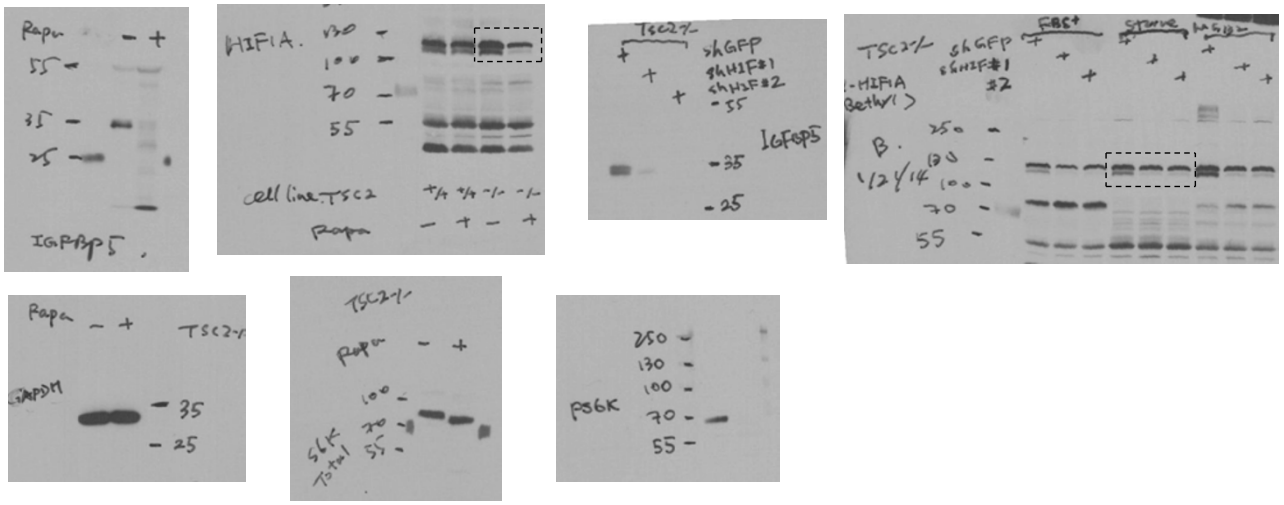

Supplementary Figure 6 continued

2.D

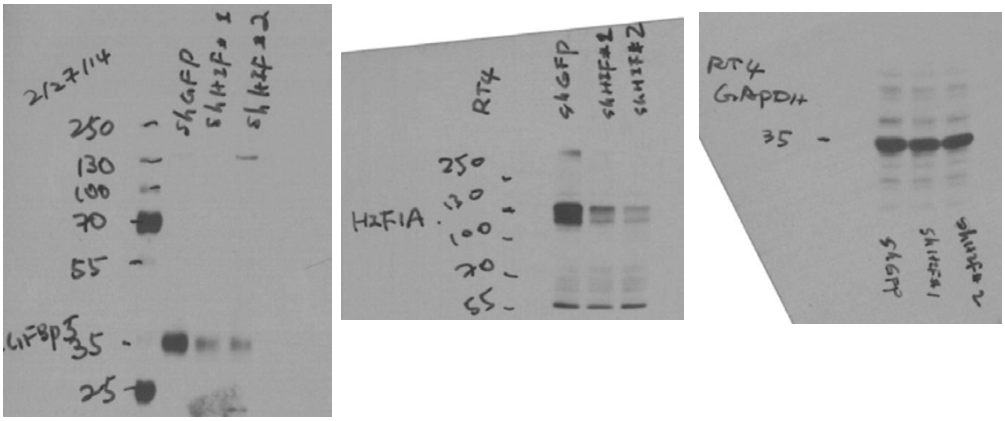

2.E

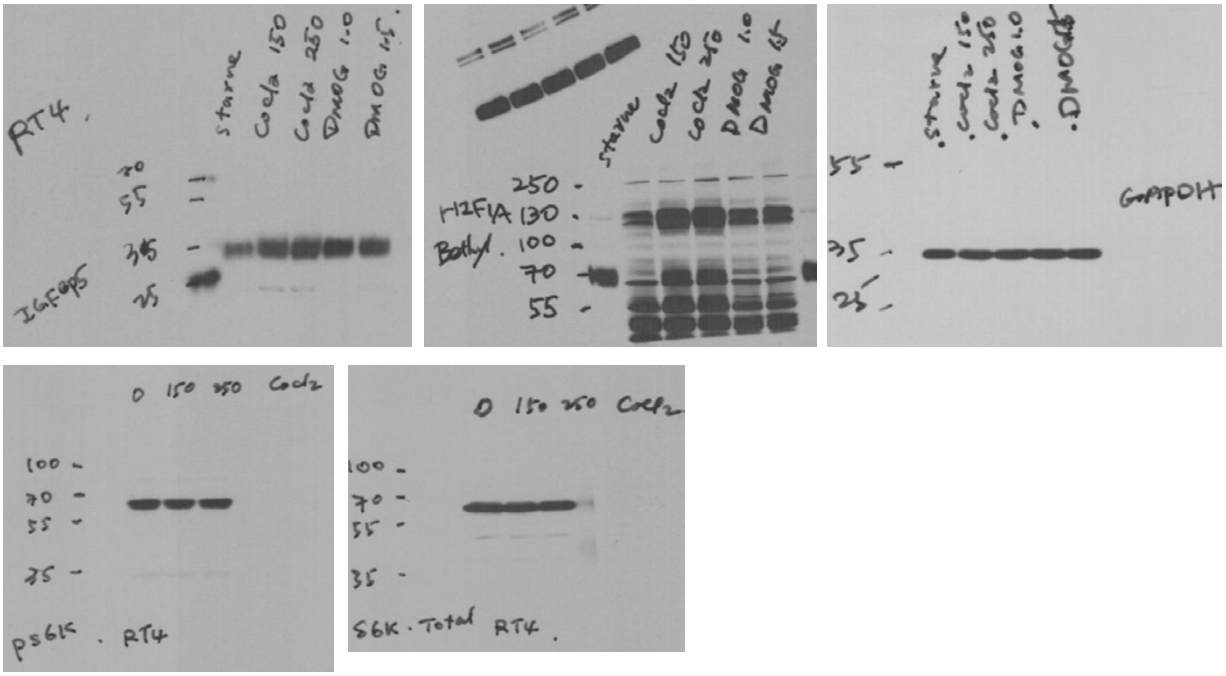

Supplementary Figure 6 continued

Figure 3

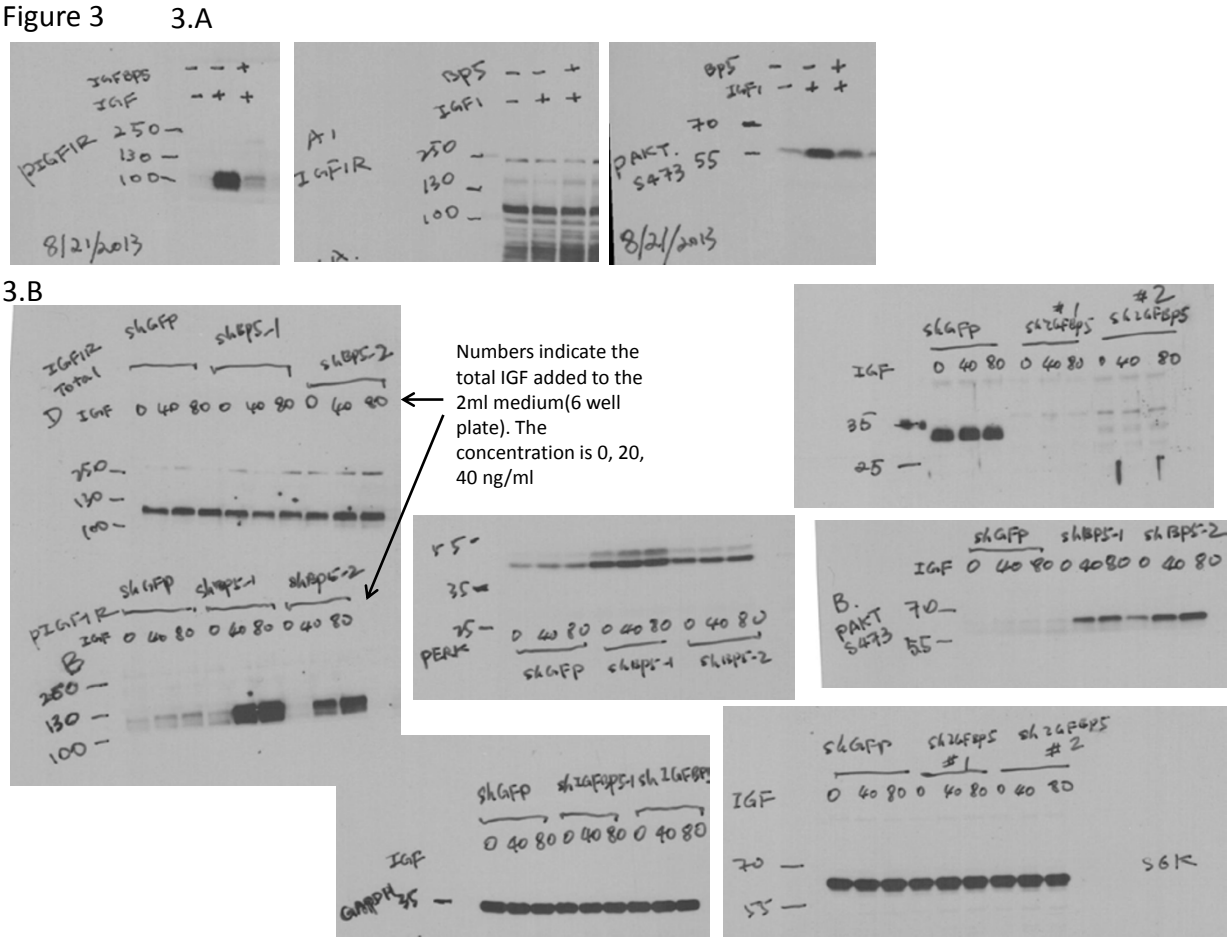

Supplementary Figure 6 continued

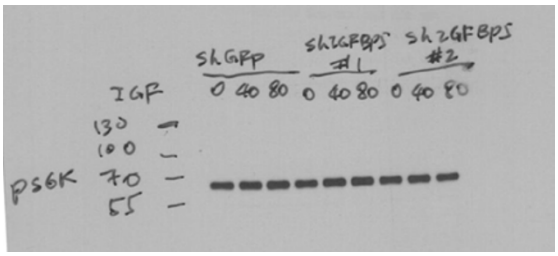

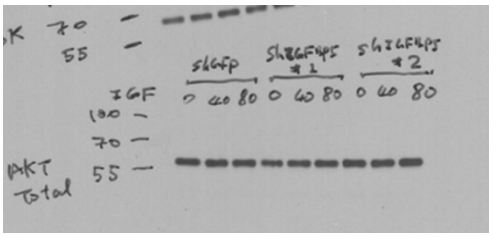

3.F

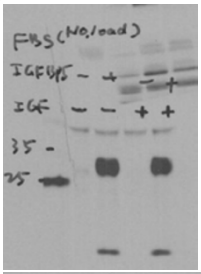

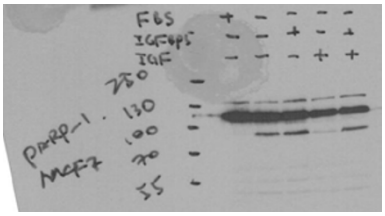

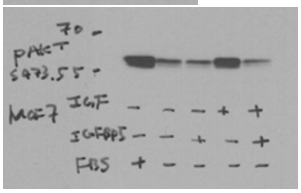

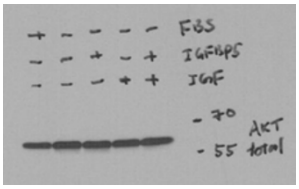

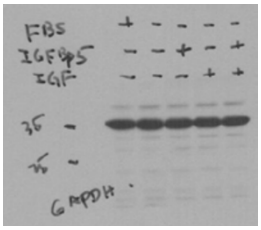

3.G

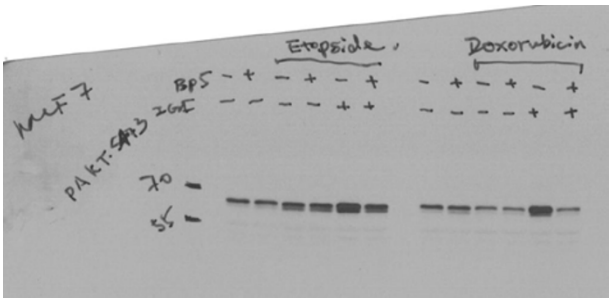

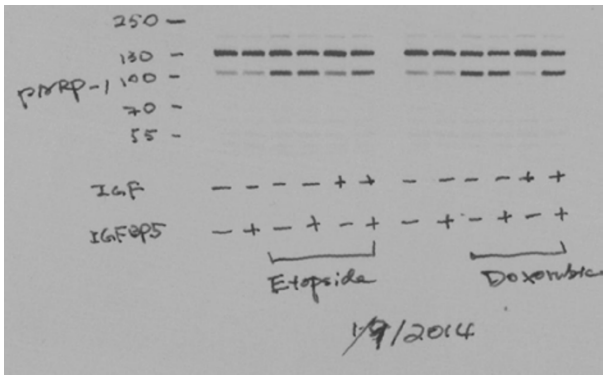

Supplementary Figure 6 continued

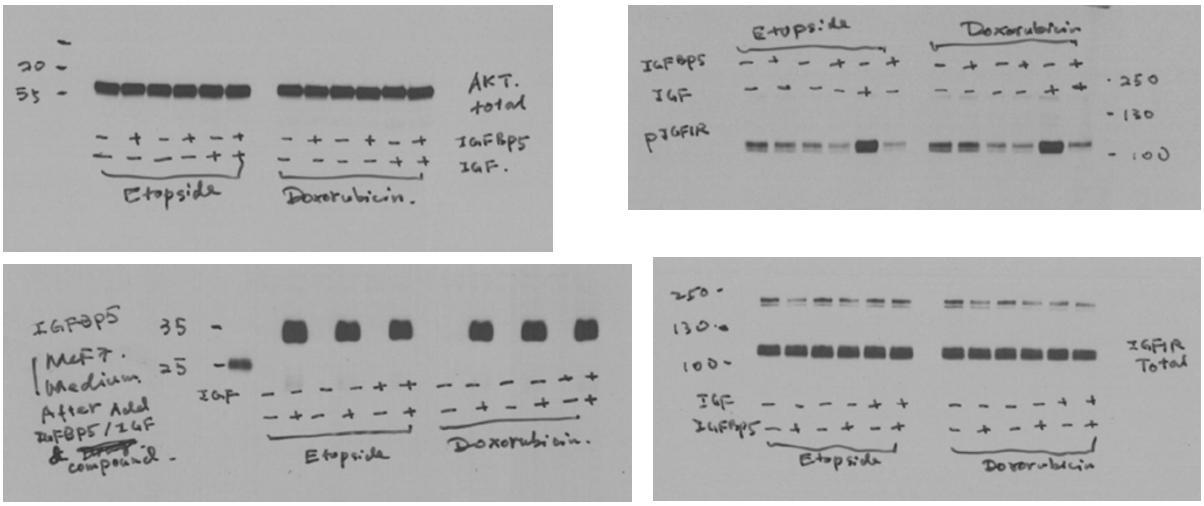

Figure 4 4.A

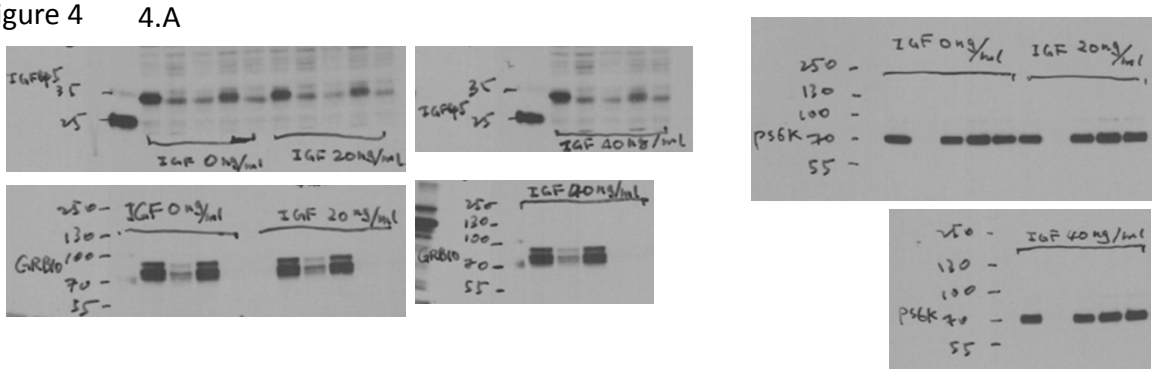

Supplementary Figure 6 continued

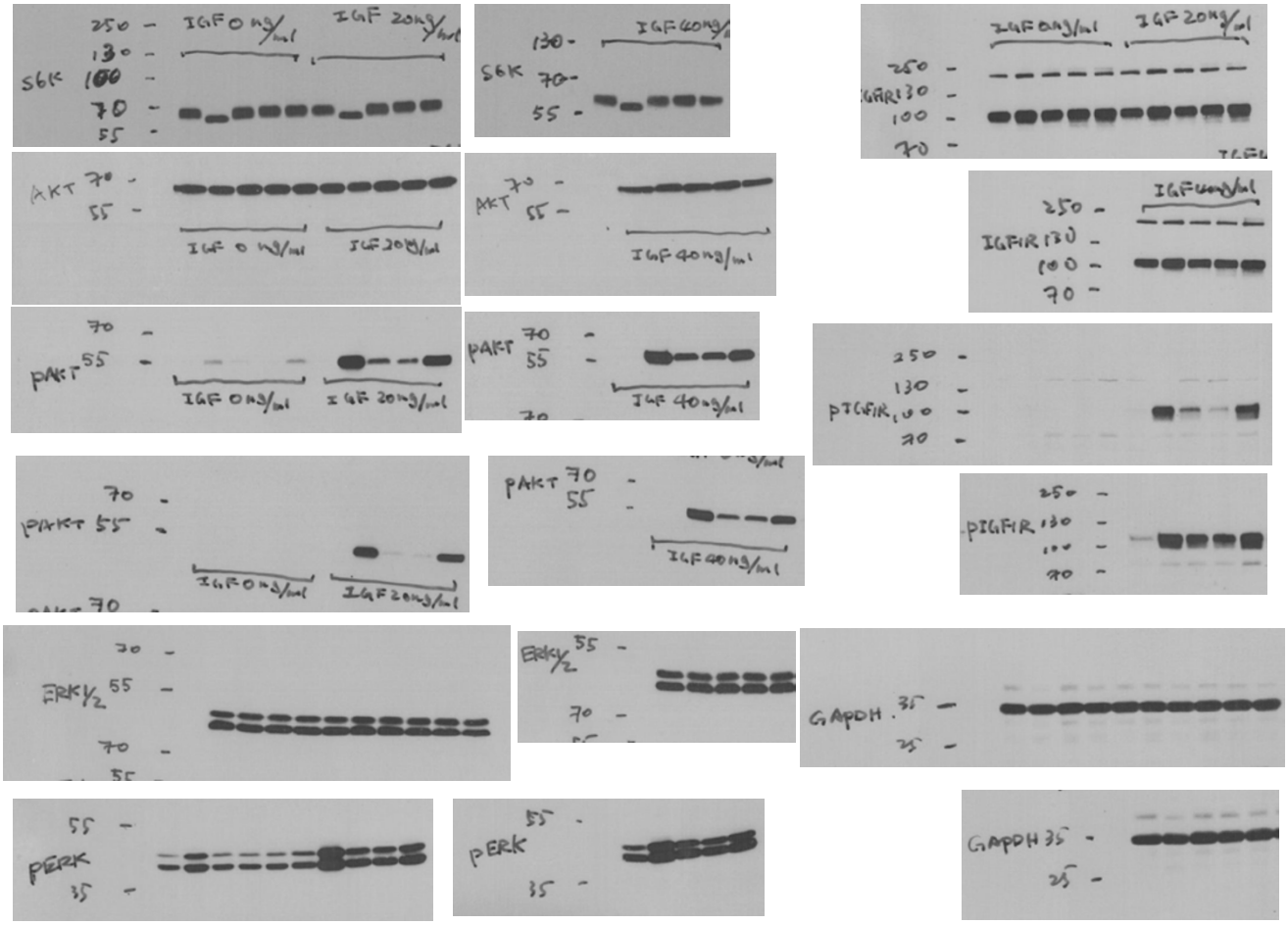

Supplementary Figure 6 continued

4.D

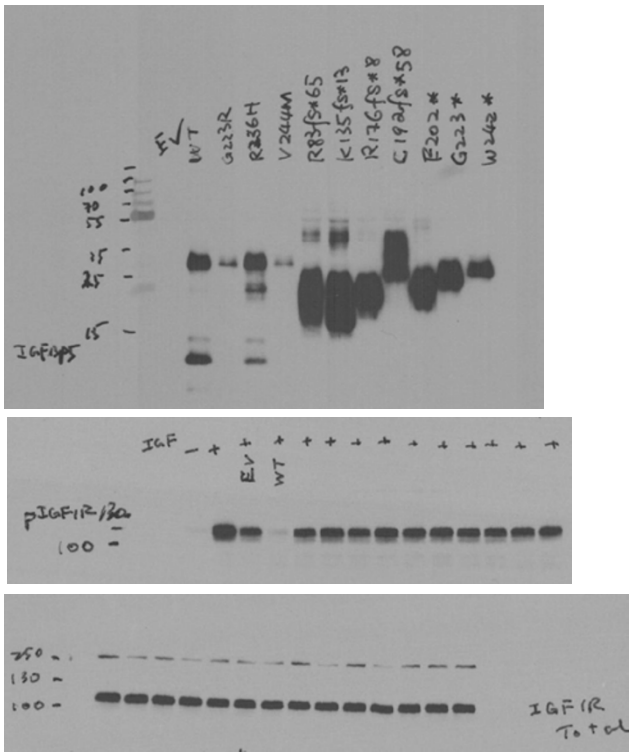

4.E

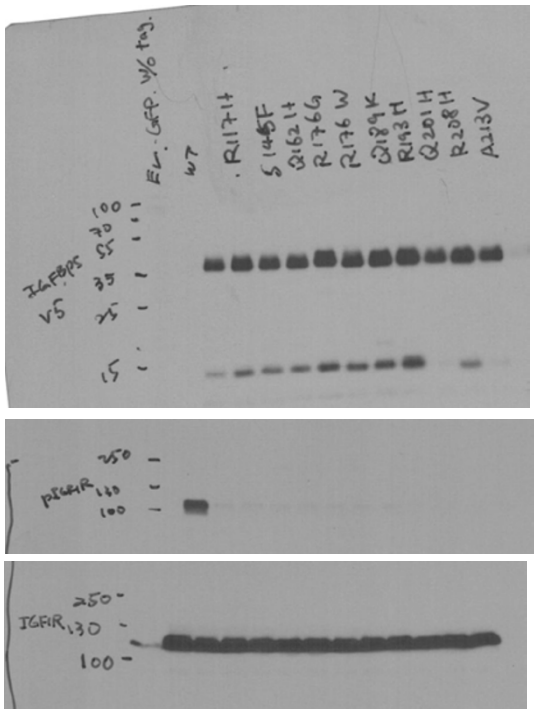

Supplementary Figure 6 continued

Supplementary Figure S4 S4.D

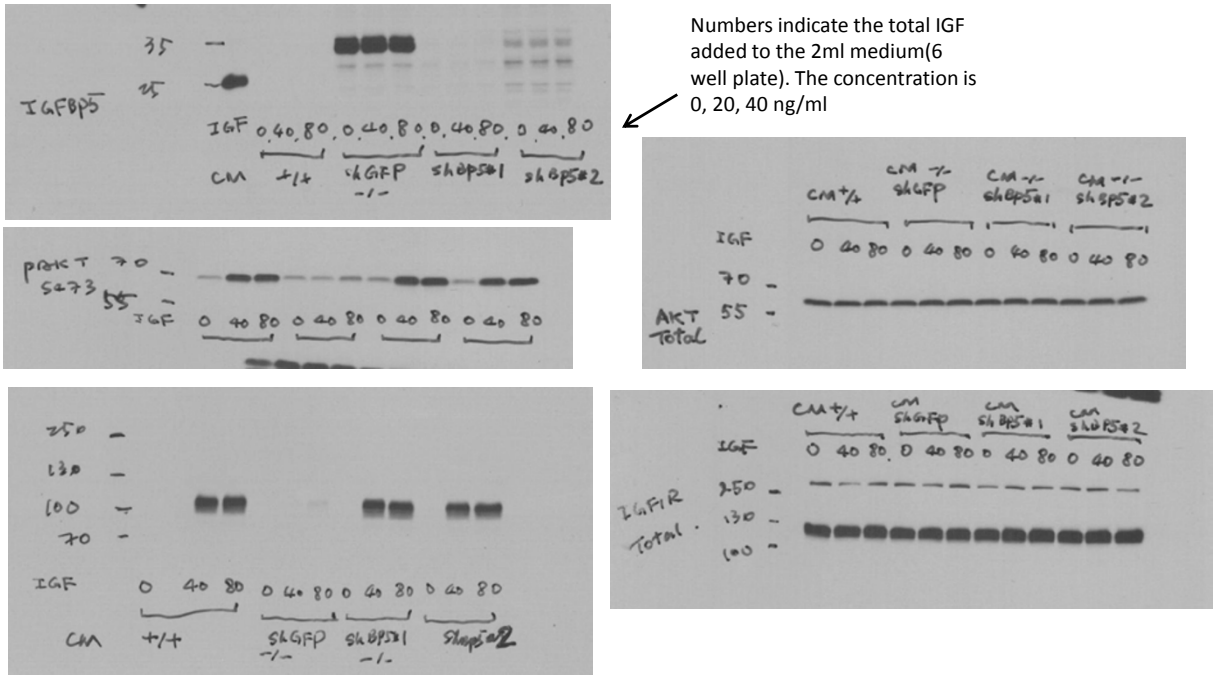

Numbers indicate the total IGF added to the 2ml medium(6 well plate). The concentration is 0, 20, 40 ng/ml

Supplementary Figure 6 continued

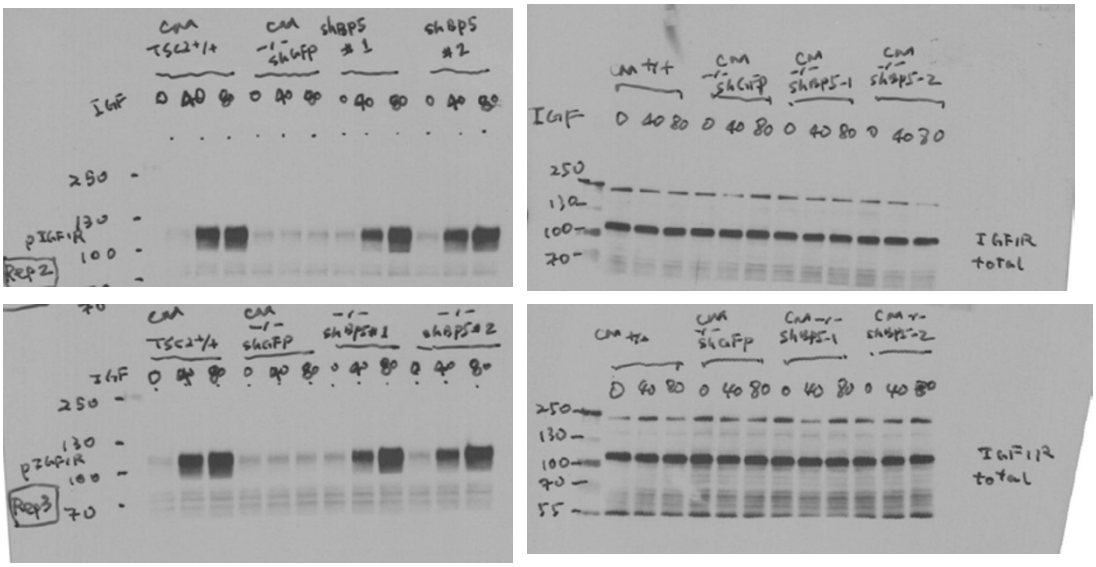

S4.E

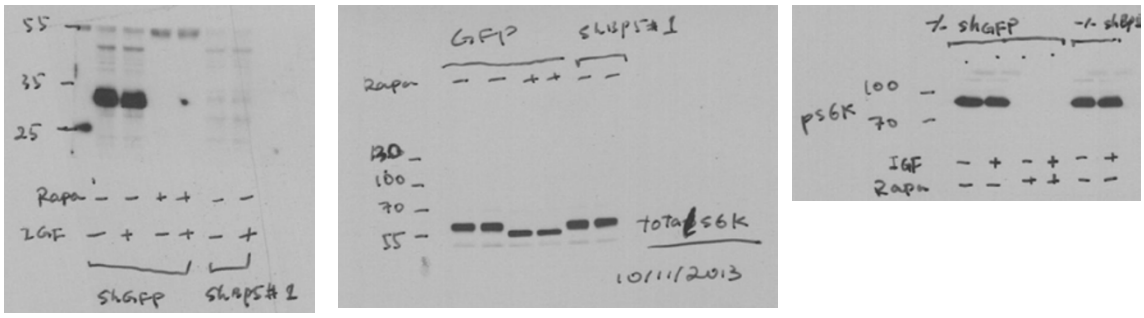

Supplementary Figure 6 continued

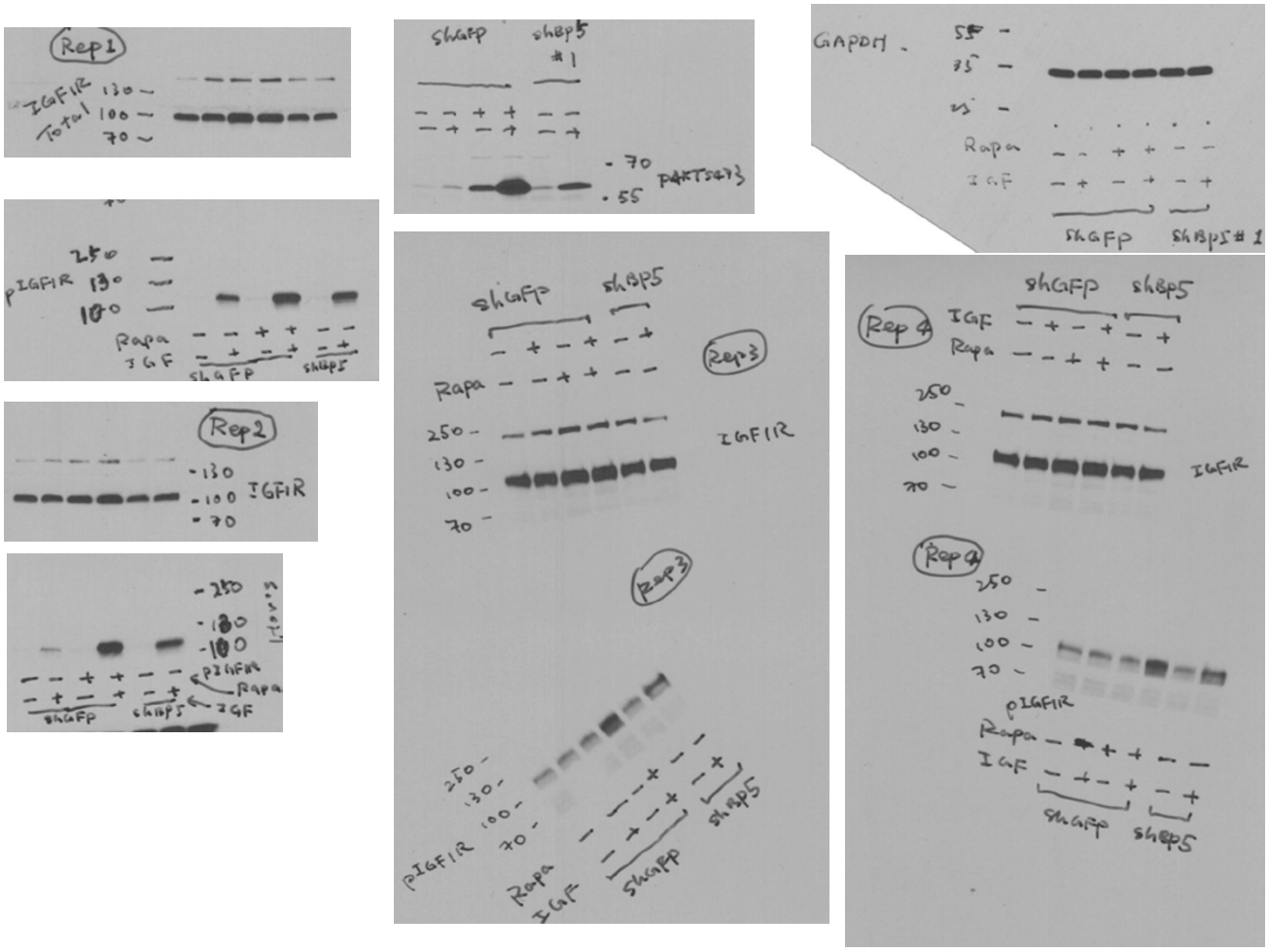

Supplementary Figure 6 continued

Supplementary Table Legends

Supplementary Table 1 Primer Sequences for qPCR

Supplementary Table 2 Primers for Luciferase Constructs

Supplementary Table 3 Primers for ChIP

Supplementary Table 4 The raw quantitative secretomic results for the experiment as described in Fig 1D. The data is uploaded in a separate excel file, with the heading annotation shown in the first tab of the excel file.

Supplementary Table 5 Representitive rapamycin-sensitive secreted proteins.

Supplementary Table 6 Rapamycin-sensitive secreted proteins sorted by relative abundances.

Supplementary Table 7 Rapamycin-sensitive secreted proteins sorted by gene symbols.

Supplementary Table 8 A list of the cancer-associated, somatic mutations of IGFBP5.

Supplementary Table 9 shRNA sequences.